

RESEARCH PAPER



TRIM7/RNF90 promotes autophagy via regulation of ATG7 ubiquitination during *L. monocytogenes* infection

Jie Wang^{a,b*}, Xiao Qin^{a,b*}, Yulu Huang^{a,b*}, Qunmei Zhang^c, Jinyong Pei^{a,b}, Yi Wang^{a,b}, Idan Goren^{d,e}, Shujun Ma^{a,b}, Zhishan Song^{a,b}, Yanzi Liu^f, Hongxia Xing^g, Hui Wang^{a,b}, and Bo Yang^{a,b}

^aHenan Key Laboratory of Immunology and Targeted Drug, Xinxiang Medical University, Xinxiang, Henan, China; ^bHenan Collaborative Innovation Center of Molecular Diagnosis and Laboratory Medicine, School of Laboratory Medicine, Xinxiang Medical University, Xinxiang, Henan, China; ^cClinical Laboratory, The First Affiliated Hospital of Xinxiang Medical University, Weihui, County, China; ^dSackler Faculty of Medicine, Tel Aviv University, Tel Aviv, Israel; ^eDepartment of Inflammation and Immunity, Lerner Research Institute, Cleveland Clinic, Cleveland, Ohio, USA; ^fDepartment of Laboratory Medicine, the Third Affiliated Hospital of Xinxiang Medical University, Xinxiang, Henan, China; ^gXinxiang Key Laboratory of Movement Disorders, The Third Affiliated Hospital of Xinxiang Medical University, Xinxiang, Henan, China

ABSTRACT

L. monocytogenes is a widely used infection model for the research on pathogenesis and host defense against gram-positive intracellular bacteria. Emerging evidence indicates that posttranslational modifications play a critical role in the regulation of macroautophagy/autophagy. However, little is known about the posttranslational modifications of ATG7, the essential protein in the autophagy process. In this study, we demonstrated that the RING-type E3 ligase TRIM7/RNF90 positively regulated autophagosome accumulation by promoting the ubiquitination of ATG7 at K413, thereby affecting *L. monocytogenes* infection. TRIM7 expression was induced by a variety range of conditions, including starvation, rapamycin stimulation, and *L. monocytogenes* infection. TRIM7 deficiency in mice or cells resulted in elevated innate immune responses and increased *L. monocytogenes* infection. ATG7 was associated with TRIM7 and the positive regulatory role of TRIM7 in *L. monocytogenes* infection-, starvation- or rapamycin-induced autophagosome accumulation was suggested by TRIM7 deficiency, TRIM7 overexpression, and TRIM7 knockdown. Further mechanistic investigation indicated that TRIM7 promoted the K63-linked ubiquitination of ATG7 at K413 and ubiquitination at this site was required for the function of ATG7 in autophagy and *L. monocytogenes* infection. Thus, our findings suggested a new regulator in intracellular bacterial infection and autophagy, with a novel posttranslational modification targeting ATG7. This research may expand our understanding of host anti-bacterial defense and the role of autophagy in intracellular bacterial infection.

Abbreviations: ATG3: autophagy related 3; ATG5: autophagy related 5; ATG7: autophagy related 7; ATG10: autophagy related 10; ATG12: autophagy related 12; ATG16L1: autophagy related 16 like 1; Baf A1: bafilomycin A; CQ: chloroquine; BMDC: bone marrow-derived dendritic cell; BMDM: bone marrow-derived macrophage; CFUs: colony-forming units; CXCL10/IP-10: C-X-C motif chemokine ligand 10; EBSS: Earle's balanced salt solution; ELISA: enzyme-linked immunosorbent assay; IFIT1/ISG56: interferon induced protein with tetratricopeptide repeats 1; IFNB/IFN- β : interferon beta; IL6: interleukin 6; IRF3, interferon regulatory factor 3; *Lm*: *L. monocytogenes*; MAP1LC3/LC3: microtubule associated protein 1 light chain 3; MEF: mouse embryonic fibroblast; MOI: multiplicity of infection; PLA: proximity ligation assay; PMA: phorbol myristate acetate; PMA-THP1, PMA-differentiated THP1; PMs: peritoneal macrophages; PTMs: posttranslational modifications; STING1, stimulator of interferon response cGAMP interactor 1; TBK1, TANK binding kinase 1; TNF/TNF- α : tumor necrosis factor; TRIM7/RNF90: tripartite motif containing; Hainan Provincial Natural Science Foundation of China.

ARTICLE HISTORY

Received 21 August 2022
Revised 21 December 2022
Accepted 21 December 2022

KEYWORDS

Autophagosome accumulation; autophagy-related genes; intracellular bacteria; posttranslational modification; ring finger proteins; E3 ligase

Introduction


Macroautophagy, hereafter called autophagy, is a fundamental biological process that contributes to cellular homeostasis by targeting cytoplasmic materials for a lysosome-dependent cellular degradation [1,2]. The initiation of autophagy can be induced by a variety of stress conditions, including nutrient starvation, energy deprivation, infection, and hypoxia [1]. Intracellular macromolecules, organelles, and invading pathogens that

are captured and targeted for autophagic destruction are sequestered into double-membrane vesicles called autophagosomes and then delivered to the lysosome for clearance [3].

Listeria monocytogenes (*L. monocytogenes*), a gram-positive intracellular bacteria, is a food-borne pathogen capable of infecting humans and other animal species. It leads to gastroenteritis that might be complicated by bacteremia and central nervous system infection which is associated with up to 30% mortality [4]. In

CONTACT Bo Yang  byang94@xxmu.edu.cn; Jie Wang  jiewang618@xxmu.edu.cn; Hui Wang  wanghui@xxmu.edu.cn  Henan Key Laboratory of Immunology and Targeted Drug, Xinxiang Medical University, Xinxiang

*These authors contributed equally to this work.

 Supplemental data for this article can be accessed online at <https://doi.org/10.1080/15548627.2022.2162706>

research, *L. monocytogenes* is considered an infection model for gram-positive intracellular bacteria and is extensively used in the laboratory to study bacterial pathogenesis and host defense [5]. It has been clear that *L. monocytogenes* induces an autophagic response, which targets *L. monocytogenes* in listeriolysin O (LLO)-damaged phagosomes and also in the cytosol under some experimental conditions [6]. Although *L. monocytogenes* is thought to evolve mechanisms to evade autophagic cellular surveillance, it has been reported that autophagy limits its intracellular growth in the early phase of primary infection [7]. In accordance with this, mice with macrophages- and granulocyte-specific deletion exhibited increased susceptibility to infection with *L. monocytogenes*, indicating the involvement of autophagy in bacterial infections [8].

It is well established that autophagy is orchestrated by several Atg (autophagy related) proteins, including Atg1 to Atg10, Atg12 to Atg14, Atg16 to Atg18, Atg29, and Atg31, which are essential for the formation of canonical autophagosomes [9]. Accumulating evidence well demonstrates that posttranslational modifications (PTMs) play a pivotal role in cellular processes [10]. In autophagy, PTMs, such as ubiquitination, phosphorylation, and acetylation, are widely involved in the exquisite regulation of autophagy in a timely and efficient way [11]. Recently, emerging evidence has identified ubiquitination as an important regulatory mechanism for the initiation, execution, and termination of autophagy [12]. Ubiquitination is the covalent conjugation of ubiquitin to the substrates through a series of enzymes, including E1 ubiquitin-activating enzyme, E2 ubiquitin-conjugating enzymes, and E3 ubiquitin-protein ligases [13]. Among these three types of enzymes, E3 ubiquitin-protein ligases determine the high substrate specificity for protein ubiquitination [14]. Generally, E3 ubiquitin-protein ligases can be divided into three main groups, HECT-, RING-, and RBP-type [15,16]. Several RING-type E3 ubiquitin-protein ligases have been demonstrated in the regulation of autophagy. For example, TRIM27 ubiquitinates ULK1 directly for proteasomal turnover to maintain control over basal ULK1 levels or catalyzes the ubiquitination of STK38L to inhibit ULK1-mediated autophagy [17]. Another RING-type E3 ligase, RNF216, interacts with BECN1 (beclin 1) and promotes its K48-linked ubiquitination, which contributes to BECN1 degradation and the inhibition of autophagy [18]. However, most of the identified modifications by ubiquitination in autophagy are targeting ULK1 or BECN1, and little is known about the regulation of other ATG proteins by ubiquitination.

In this study, we identified for the first time a pivotal role for TRIM7 (tripartite motif containing 7)-mediated ubiquitination of ATG7 in autophagy and clearance of *L. monocytogenes*. TRIM7, is a recognized RING-type E3 ubiquitin-protein ligase, involved in the development, progression, and metastasis of cancers, enterovirus replication, and TLR4-mediated innate response [19–24]. Our previous research work has demonstrated that TRIM7 plays an important role in innate immune responses against invading pathogens. TRIM7 inhibits DNA virus-triggered innate immune responses by promoting K48-linked ubiquitination and subsequent degradation of STING1, whereas TRIM7 targets MAVS for degradation and negatively regulates antiviral responses against RNA virus [25,26]. However, the role of TRIM7 in the clearance of intracellular bacteria remains unclear. We showed here that TRIM7 promoted the K63-linked ubiquitination of ATG7 at lysine residues 413 under a variety of conditions and

positively regulates autophagy. TRIM7 was induced by diverse autophagy activation conditions, including starvation, rapamycin stimulation, and *L. monocytogenes* infection. *Trim7*-deficient mice and cells showed increased susceptibility to *L. monocytogenes* infection, with enhanced innate immune response. Further study indicated that TRIM7 promoted the accumulation of autophagosomes during starvation, rapamycin stimulation, or *L. monocytogenes* infection. Collectively, our findings suggest a new regulatory role of TRIM7 in autophagy and host defenses against intracellular bacteria.

Results

TRIM7 deficiency promotes IFN β production but reduces the survival rate in mice following *L. monocytogenes* infection *in vivo*

L. monocytogenes induces IFN β /IFN- β expression through a STING1-dependent pathway [27]. Our previous research work indicated TRIM7 negatively regulates DNA virus- or cytosolic DNA-triggered signaling pathways by promoting the degradation of STING1 [26]. Thus, we wondered whether TRIM7 played a role during the process of *L. monocytogenes* infection. Firstly, we examined the expression pattern of TRIM7 upon *L. monocytogenes* infection. As shown in Figure 1a, TRIM7 expression increased in protein levels 4 h after *L. monocytogenes* infection and reached the peak at 8 h in bone marrow-derived macrophages (BMDMs), suggesting that a relationship existed between TRIM7 expression and *L. monocytogenes* infection. Next, we used *trim7*-deficient mice to investigate the role of TRIM7 in *L. monocytogenes* infection. Compared to wild-type mice, *trim7*-deficient mice exhibited a lower survival rate following *L. monocytogenes* infection (Figure 1b). Serum and various organs were collected for the measurement of type I interferon production. As shown in Figure 1c, the induction of IFN β by *L. monocytogenes* infection was enhanced in the serum of *trim7*-deficient mice. Consistently, *trim7* deficiency upregulated IFN β expression in the liver, lung, and spleen following *L. monocytogenes* infection (Figure 1d). In addition, in both the liver and spleen, increased *L. monocytogenes* infections were observed in *trim7*-deficient mice (Figure 1e). Taken together, these data indicate that whereas *trim7* deficiency increases the type I IFN production against *L. monocytogenes* infection *in vivo*, the resistance of *L. monocytogenes* is reduced in *trim7*-deficient mice.

TRIM7-deficiency or TRIM7 knockdown increases both bacterial infection and innate immune responses following *L. monocytogenes* infection

Next, we explored the role of TRIM7 at the cellular level. BMDMs, bone marrow-derived dendritic cells (BMDCs), and mouse embryonic fibroblasts (MEFs) were isolated and cultured from the *trim7*-deficient mice [26]. TRIM7-deficient HaCaT cell line was generated by CRISPR/Cas9 strategy [26]. Wild-type or *trim7*-deficient BMDMs, BMDCs, MEFs, and HaCaT cells were infected with *L. monocytogenes* or left untreated, with colony-forming units (CFUs) corresponding

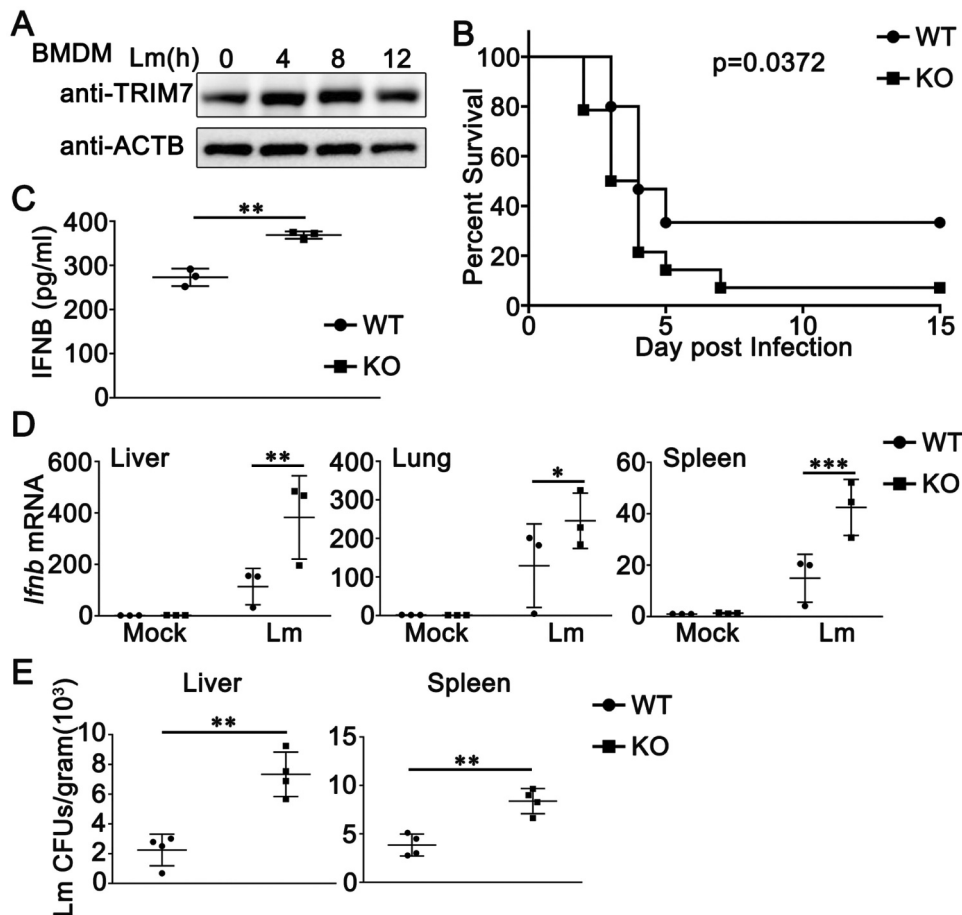


Figure 1. TRIM7 protects mice from *L. monocytogenes* infection. (A) BMDMs were stimulated with *L. monocytogenes* (*Lm*, MOI = 10) for indicated time periods. Afterward, the cells were lysed for immunoblot assays. ACTB/ β -actin was used as a loading control. (B) Wild-type (WT) and *trim7*-deficient (KO) mice ($n = 14$) were intravenously (i.v.) infected with *Lm* (1.5×10^5 CFUs/mouse). Mouse survival rates were monitored twice a day during 15 days of infection. (C) ELISA of IFNB in serum of wild-type (WT) and *trim7*-deficient (KO) mice ($n = 3$) 6 h after intravenous infection with *Lm* (1.5×10^5 CFUs/mouse). (D) Wild-type (WT) and *trim7*-deficient (KO) mice ($n = 3$) were infected with *Lm* (1.5×10^5 CFUs/mouse) for 24 h, and then the livers, lungs, and spleens of mice were subjected to real-time PCR analysis of *Ifnb* mRNA. (E) Quantification of bacterial loads in target organs (liver and spleen) from wild-type (WT) and *trim7*-deficient (KO) mice ($n = 4$) on the 3rd day after injection with *Lm* (1.5×10^5 CFUs/mouse). Bacterial loads were measured in CFUs per gram of liver (left panel) and gram of spleen (right panel). The data are representative of three independent experiments and are presented as mean \pm SD. *, $p < 0.05$, **, $p < 0.01$, ***, $p < 0.001$.

to intracellular live bacteria. Time-course analysis showed that differences in *L. monocytogenes* infection between wild-type and *trim7*-deficient BMDMs were observed in all the three time points detected, with the largest differences occurring at 6 h after infection (Figure 2a). Thus, 6 h was used in the following experiments and the increase in *L. monocytogenes* infection caused by *trim7* deficiency was confirmed in BMDMs, MEFs, and HaCaT cells (Figure 2b and Figure S1a). Next, wild-type and *trim7*-deficient MEFs or HaCaT cells were infected with *L. monocytogenes* or left uninfected and then imaged by confocal microscopy. The red dots indicated *L. monocytogenes* infection as suggested by an antibody against *L. monocytogenes*. Compared to that in wild-type cells, more red dots were detected in *trim7*-deficient MEFs and HaCaT cells, suggesting *trim7* deficiency promoted *L. monocytogenes* infection (Figure 2c, S1b, and S1c). Similarly, flow cytometry using the same antibody against *L. monocytogenes* revealed the enhancement of *L. monocytogenes* infection by *trim7* deficiency in MEFs (Figure S1D). Meanwhile, the host innate immune responses against *L. monocytogenes* infection were examined. During

L. monocytogenes infection, increased production of IFNB, CXCL10/IP-10, IFIT1/ISG56, and TNF/TNF- α was observed in RNA90-deficient BMDMs (Figure 2d). Consistently, *Trim7* deficiency in HaCaT cells enhanced the production of IFNB and CXCL10 upon *L. monocytogenes* infection (Figure S1E). In peritoneal macrophages (PMs), *trim7* deficiency resulted in elevated phosphorylation levels of TBK1, IRF3, and RELA/p65 after *L. monocytogenes* infection (Figure 2e). Upon *L. monocytogenes* infection, compared to wild-type PMs, *trim7*-deficient PMs exhibited higher levels of IFNB in ELISA assays (Figure 2f). To further evaluate the role of TRIM7 in *L. monocytogenes* infection, bacterial entry and *L. monocytogenes* triggered innate immune responses were investigated in TRIM7-silenced phorbol-12-myristate-13-acetate (PMA)-differentiated THP1 (PMA-THP1, a human macrophage-like cell line) cells. TRIM7 was silenced by TRIM7-specific siRNA R3, the efficiency of which had been proved in our previous research [26]. As shown in Figure 2g, an increased bacterial load of *L. monocytogenes* was observed in TRIM7-silenced cells. At the same time, TRIM7 knock-down enhanced *L. monocytogenes*-induced innate immune

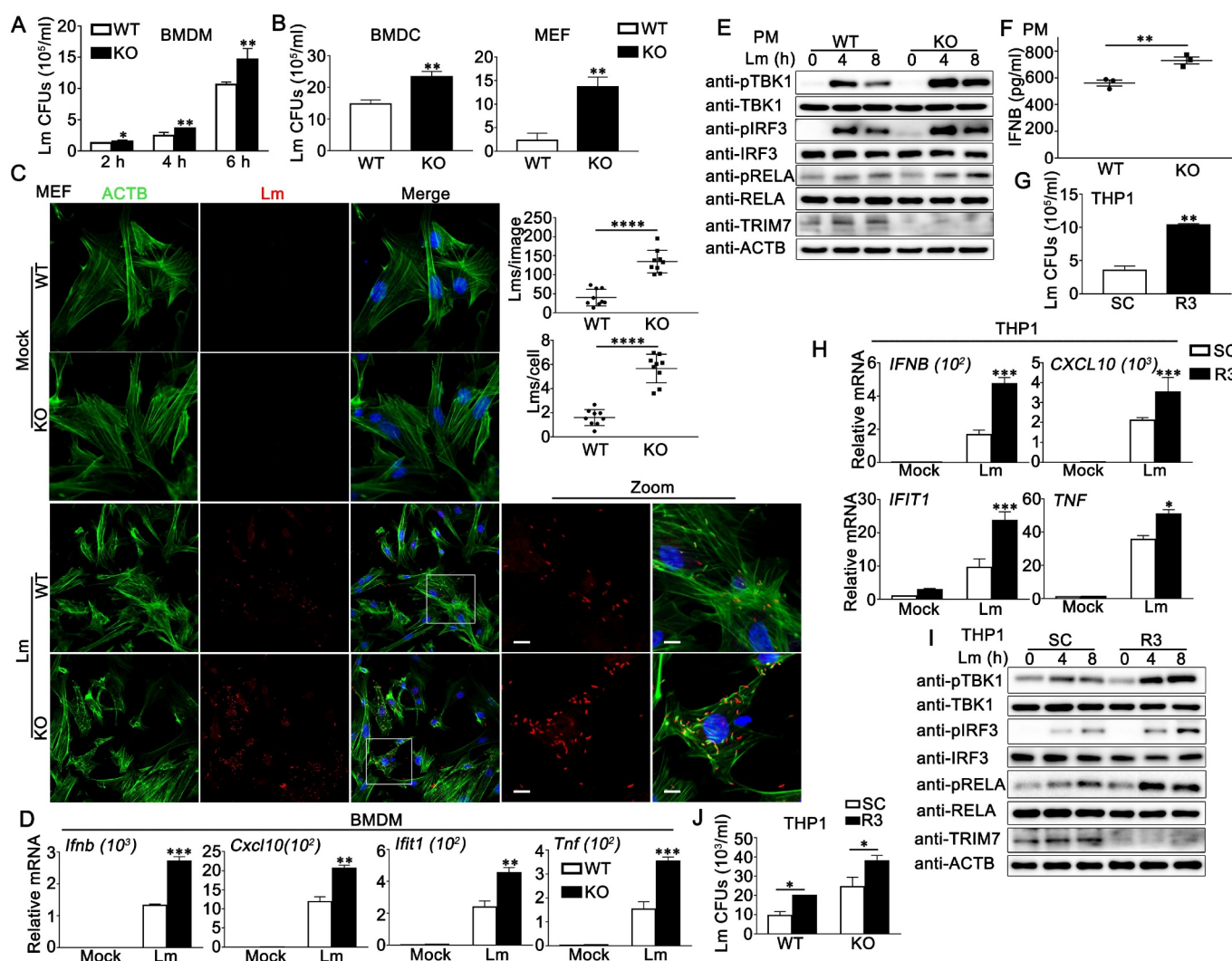


Figure 2. TRIM7 negatively regulated *Lm* infection in cells. (A) CFUs obtained at indicated time points from wild-type (WT) and *trim7*-deficient (KO) BMDMs infected with *L. monocytogenes* (*Lm*) (MOI = 10). (B) CFUs obtained at 6 h from wild-type (WT) and *trim7*-deficient (KO) BMDCs (left panel) or MEFs (right panel) infected with *L. monocytogenes* (*Lm*) (MOI = 10). (C) Confocal microscopy images of *Lm*-infected wild-type (WT) and *trim7*-deficient (KO) MEFs at 6 h after infection. The left panel shows DAPI (blue), *Lm* (red), ACTB (green), and merged views of three channels. The bottom right panel shows magnified views of the boxed areas from the merged view. Yellow indicates the co-localization of *Lm* with ACTB. Scale bars: 10 μ m (magnified views). The top right panel shows the statistical analysis of the total number of bacteria and the number of bacteria per cell in all pictures (9 pictures per genotype). (D) Wild-type (WT) and *trim7*-deficient (KO) BMDMs were infected with *Lm* for 8 h, and then subjected to real-time PCR analysis. (E) Wild-type (WT) and *trim7*-deficient (KO) PMs were infected with *Lm* (MOI = 10) for indicated time periods. Afterward, the cells were lysed for immunoblot assays. (F) Wild-type (WT) and *trim7*-deficient (KO) PMs were infected with *Lm* (MOI = 10) for 24 h. The secretion of IFN β was measured by ELISA. (G) PMA-THP1 cells were transfected with control siRNA (SC) or TRIM7-specific siRNA (R3). At 24 h after transfection, the cells were infected with *Lm* (MOI = 10) for 6 h, and then colony forming assay was performed. (H) PMA-THP1 cells were transfected with control siRNA (SC) or TRIM7-specific siRNA (R3). At 24 h after transfection, the cells were infected with *Lm* (MOI = 10) for 8 h and then subjected to real-time PCR analysis. (I) PMA-THP1 cells were transfected with control siRNA (SC) or TRIM7-specific siRNA (R3). At 24 h after transfection, the cells were infected with *Lm* (MOI = 10) for indicated time periods. Afterward, the cells were lysed for immunoblot assays. (J) Wild-type (WT) or STING1-deficient (KO) PMA-THP1 cells were transfected with control siRNA (SC) or TRIM7-specific siRNA (R3). At 24 h after transfection, the cells were infected with *Lm* (MOI = 10) for 6 h, and then colony forming assay was performed. The data are representative of three independent experiments and are presented as mean \pm SD. *, $p < 0.05$, **, $p < 0.01$, ***, $p < 0.001$, ****, $p < 0.0001$.

responses, including the production of IFN β , CXCL10, IFIT1, and TNF (Figure 2h) and the phosphorylation of TBK1, IRF3, and RELA (Figure 2i). Finally, considering that TRIM7 regulated STING1-mediated innate immune responses [26], we examined whether the inhibitory role of TRIM7 in *L. monocytogenes* infection was dependent on STING1. Wild-type or STING1-deficient PMA-THP1 cells were transfected with control siRNA (SC) or TRIM7-specific siRNA (R3) and CFUs were obtained after transfection. As shown in Figure 2j, although STING1 deficiency resulted in elevated *L. monocytogenes* infection, it did not make a significant change in the enhancement in *L. monocytogenes* infection

caused by TRIM7 knockdown, suggesting TRIM7 negatively regulated *L. monocytogenes* infection independent on STING1. Taken together, all these findings suggest that both *L. monocytogenes* infection and innate immune responses are enhanced by TRIM7 deficiency or TRIM7 knockdown.

TRIM7 interacts with ATG7

TRIM7 deficiency promoted *L. monocytogenes* infection with elevated innate immune responses and in a STING1-independent way, suggesting that other mechanisms existed for the regulation of *L. monocytogenes* infection. We wondered whether TRIM7

colocalized with or modified the bacterial surface directly. Flag-TRIM7 was transfected into *trim7*-deficient MEFs and then infected with *L. monocytogenes*. However, no significant colocalization between TRIM7 and *L. monocytogenes* was observed, indicating it was unlikely that TRIM7 modified the bacterial surface directly (Figure S1F). Then, to explore the underlying mechanism by which TRIM7 regulated *L. monocytogenes* infection, we tried to identify the potential substrate of TRIM7 by co-immunoprecipitation. HEK293T cells were transfected with or without Flag-TRIM7 and then subjected to immunoprecipitation with an anti-Flag antibody. The immunoprecipitates were sent for mass spectroscopy analysis and a few proteins were identified as potential TRIM7-associated proteins (Figure 3a). ATG7, which has been reported to be a core autophagy-related protein that is indispensable to classical autophagy [28], was identified to be associated with TRIM7 (Figure 3a). To investigate the association between TRIM7 and ATG7, Flag-TRIM7 and HA-ATG7 were transfected into HEK293T cells. Subsequent co-immunoprecipitation experiments were performed and the results suggested exogenous expressed TRIM7 bound to ATG7 (Figure 3b,c). Consistently, confocal microscopy assays indicated that Flag-TRIM7 was colocalized with Cherry-ATG7 in HEK293T cells, as much overlap between the two signals at the pixel level was observed (Figure 3d). To confirm the endogenous interaction between TRIM7 and ATG7, PMA-THP1 cells were treated with *L. monocytogenes* infection, starvation with EBSS, rapamycin or left untreated and then subjected to co-immunoprecipitation analysis. As shown in Figures 3e,f, endogenous TRIM7 interacted with ATG7 in untreated PMA-THP1 cells and more TRIM7-ATG7 interaction was observed after *L. monocytogenes* infection, starvation, or rapamycin stimulation, which might be caused at least partly by the increased expression of TRIM7. In addition, we performed *in situ*-proximity ligation assay (PLA) to validate the TRIM7-ATG7 interaction. *Trim7*-deficient MEFs were transfected with Flag-TRIM7 and then left uninfected or infected with *L. monocytogenes*. PLA was performed using anti-Flag and anti-ATG7 antibodies. The detected red dots depicted the colocalization of TRIM7 and ATG7. As shown in Figure 3g, the red dots indicating TRIM7-ATG7 interaction were detected in untreated cells and more red dots were observed after *L. monocytogenes* infection. Next, we explored the region of TRIM7 responsible for its interaction with ATG7. Surprisingly, co-immunoprecipitation assays indicated only the full-length TRIM7 interacted with ATG7 (Figure 3h,i). We also mapped the binding regions on ATG7 for the TRIM7 association. As shown in Figure 3j,k, only very weak interaction was detected between the C-terminal domain (CTD) or N-terminal domain (NTD) of ATG7 and TRIM7. In all, our findings suggest that TRIM7 interacts with ATG7.

TRIM7 promotes *L. monocytogenes*-triggered autophagy

Given that TRIM7 interacted with ATG7, the protein essential to autophagy, and autophagy plays an important role in host defense against intracellular bacteria, we proposed the hypothesis that TRIM7 regulates autophagy targeting ATG7. To test our hypothesis, the effect of TRIM7 overexpression on *L. monocytogenes*-induced autophagy was evaluated by LC3-II levels in immunoblot assays. As shown in Figure 4a,b, TRIM7 overexpression in HeLa

cells resulted in enhanced LC3-II accumulation in a dose-dependent pattern during *L. monocytogenes* infection. In addition, to distinguish between effects on autophagosome accumulation and degradation, we pretreated the cells with bafilomycin A₁ (Baf A1), which impaired lysosome activity and allowed us to assess LC3-II/autophagosome formation. TRIM7 promoted *L. monocytogenes* infection-triggered LC3-II accumulation to a similar extent with or without Baf A1, suggesting TRIM7 regulated the autophagosome formation, but not the degradation by lysosome (Figure 4b). Further, the effect of TRIM7 overexpression on *L. monocytogenes*-induced LC3-II puncta formation was examined by confocal microscopy. HeLa cells expressing mCherry-LC3 (HeLa-mCherry-LC3) were transfected with TRIM7 or a control vector, and then infected with *L. monocytogenes* or left uninfected. As shown by confocal microscopy, LC3-II puncta formation was augmented by TRIM7 overexpression (Figure 4c).

To confirm the positive regulatory role of endogenous TRIM7 in *L. monocytogenes*-induced autophagosome accumulation, *trim7*-deficient BMDCs or BMDMs were infected with *L. monocytogenes* and then the autophagosome accumulation was evaluated by LC3-II levels. Induction of LC3-II accumulation by *L. monocytogenes* infection was observed in both BMDCs and BMDMs and this induction was significantly decreased by *trim7* deficiency, suggesting TRIM7 promoted *L. monocytogenes*-triggered autophagosome accumulation (Figure 4d,e). Then, the effect of TRIM7 on LC3-II accumulation was examined *in vivo*. Wild-type or *trim7*-deficient mice were infected with *L. monocytogenes* and LC3-II accumulation in lungs and livers was detected by immunoblots. In both lungs and livers, compared to wild-type mice, *trim7*-deficient mice exhibited lower levels of LC3-II accumulation in these organs (Figure 4f). Further, we investigated the role of TRIM7 in *L. monocytogenes*-triggered autophagosome accumulation in TRIM7-deficient HaCaT cells, the generation of which had been demonstrated in our previous research [26]. As shown in Figure 4g, TRIM7 deficiency significantly decreased the LC3-II accumulation in HaCaT cells upon *L. monocytogenes* infection. Consistently, confocal microscopy analysis indicated that decreased LC3-II puncta formation was observed in TRIM7-deficient HaCaT cells than that in wild-type cells after *L. monocytogenes* infection (Figure 4h).

Finally, the effect of TRIM7 on *L. monocytogenes*-induced autophagosome accumulation was examined in TRIM7-silenced cells. TRIM7 knockdown by siRNA R3 in HeLa cells expressing mCherry-LC3 inhibited LC3-II puncta formation as suggested by confocal microscopy (Figure 4i). Consistent with these findings, LC3-II accumulation was decreased by TRIM7 knockdown via the transfection of R3 (Figure 4j). In all, the positive regulatory role of TRIM7 in *L. monocytogenes*-induced autophagosome accumulation is suggested by TRIM7 deficiency, TRIM7 overexpression, and TRIM7 knockdown.

TRIM7 promotes autophagy in the basal state and response to a variety of stress conditions

Given that TRIM7 manipulated *L. monocytogenes*-triggered autophagy, we wondered whether TRIM7 regulated the autophagy that was induced by other conditions, including nutrient starvation and rapamycin stimulation. Considering that the expression levels of TRIM7 are usually very low in rest cells and can be induced by

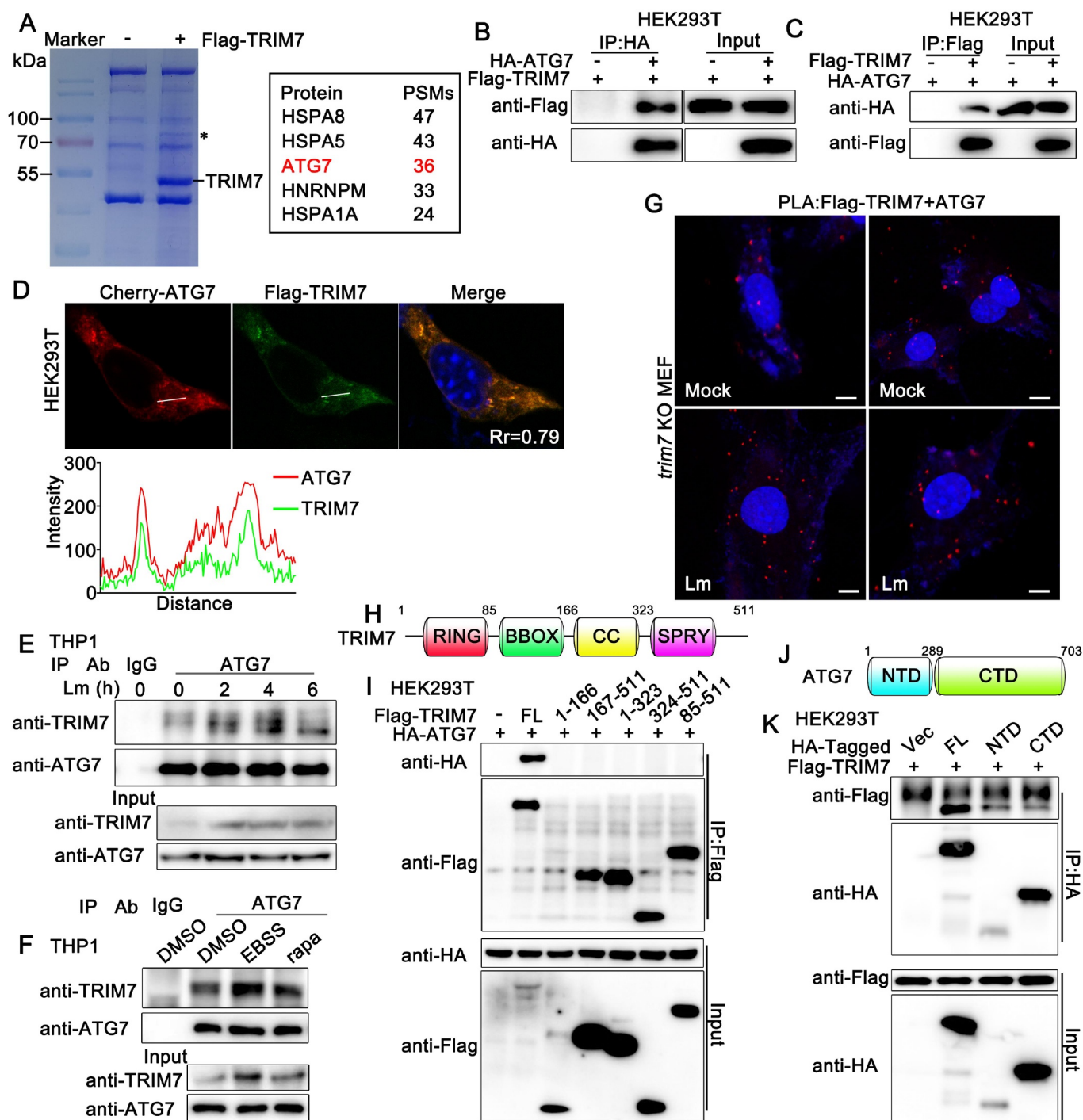


Figure 3. TRIM7 interacted with ATG7. (A) HEK293T cells were transfected with Flag-TRIM7 (+) or Vector (-) for 24 h, and then the cell lysates were subjected to immunoprecipitation with an anti-Flag antibody. The immunoprecipitates were resolved in SDS-PAGE followed by coomassie blue staining. The specific band highlighted by an asterisk was excised for mass spectrometry identification. PSMs, peptide spectrum matches. (B, C) HEK293T cells were transfected with Flag-TRIM7 and HA-ATG7. At 24 h after transfection, the cell lysates were subjected to immunoprecipitation (IP) and immunoblot (IB) analysis as indicated. (D) HEK293T cells were transfected with Flag-TRIM7 and mCherry-ATG7. At 24 h after transfection, immunofluorescence was performed using anti-Flag (green). Nuclei were stained with DAPI. Plots of pixel intensity along the white line were shown in the right panel. Pearson's correlation coefficient was calculated using ImageJ software. Rr, Pearson's correlation coefficient. (E) PMA-THP1 cells were infected with *Lm* for indicated time periods, and then the cell lysates were subjected to immunoprecipitation (IP) and immunoblot (IB) analysis as indicated. (F) PMA-THP1 cells were treated with rapamycin for 12 h or EBSS for 2 h, and then the cell lysates were subjected to immunoprecipitation (IP) and immunoblot (IB) analysis as indicated. (G) *trim7*-deficient (KO) MEFs were transfected with Flag-TRIM7. At 24 h after transfection, the cells were infected with *Lm* for 4 h or left uninfected, and then *in situ* PLA assay was performed to examine the colocalization of TRIM7 and ATG7. TRIM7-ATG7 complex, red; nuclei, blue. (H) A schematic presentation of full-length TRIM7. RING, ring-finger domain; BB, B-box domain; CC, coiled-coil domain; SPRY, SPRY domain. (I) HEK293T cells were transfected with indicated plasmids. At 24 h after transfection, the cell lysates were subjected to immunoprecipitation (IP) and immunoblot (IB) analysis as indicated. (J) A schematic presentation of full-length ATG7. NTD, N-terminal domain, 1–289aa; CTD, C-terminal domain, 290–703aa. (K) HEK293T cells were transfected with indicated plasmids. At 24 h after transfection, the cell lysates were subjected to immunoprecipitation (IP) and immunoblot (IB) analysis as indicated. The data are representative of three independent experiments.

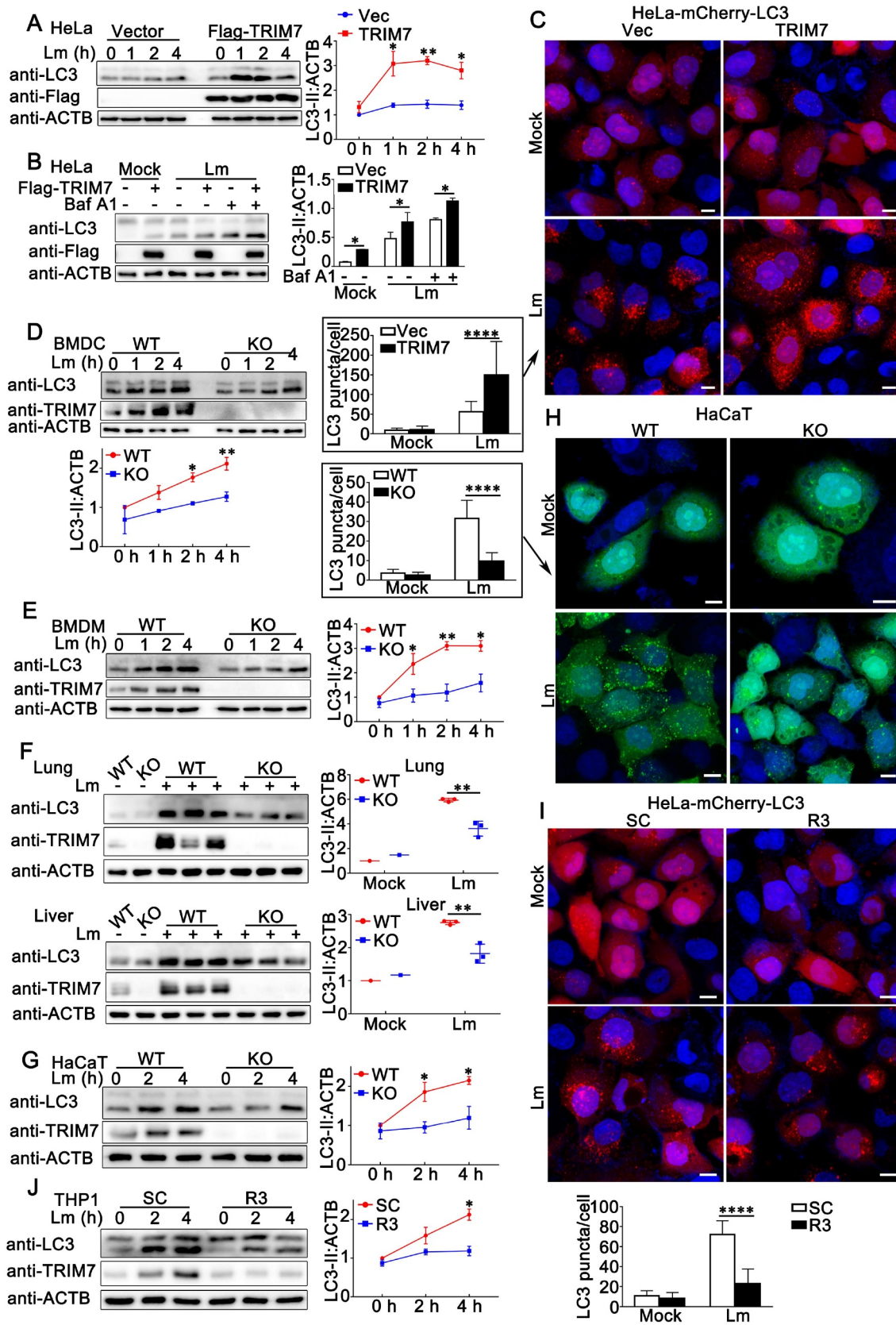


Figure 4. TRIM7 positively regulated *Lm* infection-induced autophagy. (A) HeLa cells were transfected with 0.5 μ g Vector or TRIM7 plasmid. At 24 h after transfection, the cells infected with *Lm* (MOI = 10) or PBS for indicated time periods, and then subjected to immunoblot analysis. LC3-II density was shown in the right panel. (B) HeLa cells were transfected with 0.5 μ g Vector (-) or TRIM7 (+) plasmid. At 24 h after transfection, the cells were treated with PBS, *Lm* (MOI = 10), or *Lm* with bafilomycin A₁ (400 nM) for 2 h, and then subjected to immunoblot analysis. LC3-II density was shown in the right panel. (C) HeLa-mCherry-LC3 cells were transfected with Vector (Vec) or TRIM7. At 24 h after transfection, the cells were infected with *Lm* (MOI = 10) or left uninfected for 4 h, and then subjected to confocal microscopy analysis. Scale bars: 10 μ m. LC3 puncta quantification was shown in the left panel. (D, E) Wild-type (WT) and *trim7*-deficient (KO) BMDCs (D) and BMDMs (E) were stimulated with *Lm* (MOI = 10) for the indicated time periods. Afterward, the cells were lysed for immunoblot assays (left panels). LC3-II density was shown

virus or bacterial infection, we examined the expression patterns of TRIM7 protein in these conditions. Immunoblot assays indicated that TRIM7 protein expression was induced by nutrient starvation using EBSS (Figure S2A) or rapamycin stimulation (Figure S2B) in PMA-THP1 cells. Next, HeLa cells were transfected with TRIM7 and then treated with EBSS (starvation) or rapamycin. Immunoblot assays demonstrated that TRIM7 overexpression promoted LC3-II accumulation upon starvation or rapamycin stimulation (Figure 5a,b). Using Baf A1 to inhibit lysosome activity, we found that TRIM7 enhanced the LC-II accumulation to a similar extent with or without Baf A1, an indication that TRIM7 increased autophagosome accumulation, but not lysosomal degradation upon starvation or rapamycin stimulation (Figure 5c,d). Further, in basal conditions, TRIM7 overexpression caused an increase in LC3-II levels with or without Baf A1, suggesting positive regulation of TRIM7 in autophagosome formation (Figure 5e). In addition, TRIM7 overexpression in HeLa-mCherry-LC3 significantly increased LC3-II puncta accumulation after nutrient starvation or rapamycin treatment (Figure 5f).

Then the role of TRIM7 in starvation- or rapamycin-triggered autophagosome accumulation was explored in TRIM7-deficient cells. As suggested by immunoblots, *trim7* deficiency in BMDMs, MEFs or HaCaT cells resulted in decreased LC3-II accumulation upon starvation (Figure 5g, Figure S2c, and Figure S2e) or rapamycin stimulation (Figure 5h, Figure S2d and Figure S2f), indicating that TRIM7 played a positive role in the regulation of autophagosome formation under these conditions. In addition, compared to wild-type cells, TRIM7-deficient HaCaT cells displayed lower levels of LC3-II puncta formation after stimulation with rapamycin (Figure 5i). Further, in basal condition, although the effect of TRIM7 deficiency on LC3-II levels was not significant because of the low levels of LC3-II in basal condition, TRIM7 deficiency caused a decrease in LC3-II levels in the presence of lysosomal inhibitor chloroquine (CQ) or Baf A1, suggesting positive regulation of TRIM7 in autophagosome formation (Figure 5j). Finally, TRIM7 knockdown prevented the LC3-II puncta accumulation that was triggered by nutrient starvation or rapamycin stimulation (Figure S2g). Consistently, TRIM7 knockdown impaired autophagosome formation in basal conditions (Figure S2h). Taken together, TRIM7 promotes basal autophagy and autophagy induced by a variety of stress conditions.

TRIM7 regulates ATG7-related ubiquitin-like conjugation systems in autophagy

As an E1-like enzyme, ATG7 is involved in two ubiquitin-like conjugation systems in classical autophagy, ATG12-ATG5-ATG16L1 conjugation system with ATG10 as an E2-like enzyme, and LC3-PE conjugation system with ATG3 as E2-

like enzyme [29]. Given that TRIM7 interacted with ATG7 and promoted autophagosome formation, we examined whether TRIM7 regulated ATG7-related ubiquitin-like conjugation systems in autophagy by co-immunoprecipitation. As shown in Figure 6a,b, TRIM7 overexpression promoted but TRIM7 deficiency impaired the association of ATG5 with ATG16L1 in autophagy that was triggered by *L. monocytogenes* infection. Consistently, after the treatment of starvation or rapamycin, compared to wild-type cells, TRIM7-deficient HaCaT cells exhibited decreased ATG5-ATG16L1 association (Figure 6c,d). Next, we investigated the effects of TRIM7 on the second conjugation system and found that TRIM7 overexpression resulted in enhanced LC3-ATG3 association after *L. monocytogenes* infection or rapamycin stimulation (Figure 6e,f), whereas TRIM7 deficiency impaired the LC3-ATG3 association after *L. monocytogenes* infection in both HaCaT cells and BMDMs (Figure 6g,h). In all, TRIM7 positively regulates ATG7-related ubiquitin-like conjugation systems in autophagy.

TRIM7 promoted the K63-linked ubiquitination of ATG7

Considering TRIM7 serves as an E3 ligase in several signaling pathways [19,25,26], we thought TRIM7 might have regulated the ubiquitination of ATG7. To examine this hypothesis, TRIM7 was co-transfected with ATG7 and HA-tagged ubiquitin, and the ubiquitination of ATG7 was detected by immunoprecipitation. As shown in Figure 7a, TRIM7 overexpression increased the ubiquitination of ATG7 in a dose-dependent manner. To exclude the possibility that the observed ubiquitination was on ATG7-interacting proteins, and not ATG7 itself, we performed the reverse IP and detected the modification of ATG7. As shown in Figure S3A, increased high molecular weight smears of ATG7 were observed with TRIM7 overexpression, indicating TRIM7 promoted the ubiquitination of ATG7. The activity of RING-type ubiquitin-protein ligases is dependent on their RING domains which contain conserved cysteine and histidine residues essential for recruiting the E2 ubiquitin-conjugating enzymes [30]. Our previous research indicated that the C29, 32A mutant (the integrity of the RING domain was destroyed) and the ΔR mutant (lacking RING domain) lost the ability of ubiquitination targeting STING1 [26]. Therefore, we investigated the effects of these mutants on the ubiquitination and the results suggested both C29,32A and ΔR mutants barely increased the ubiquitination of ATG7, suggesting the RING domain of TRIM7 was critical to the ubiquitination of ATG7 (Figure 7b). Ubiquitin contains seven Lys residues (K6, K11, K27, K29, K33, K48, and K63), so seven different

at the bottom (D) or right (E) panels. (F) Wild-type (WT) and *trim7*-deficient (KO) mice ($n = 3$) were intravenously (i.v.) infected with *Lm* (1.5×10^5 CFUs/mouse) or left uninfected for 2 days, then the livers and lungs of the mice were subjected to immunoblot assays. LC3-II density was shown in the right panels. (g) Wild-type (WT) and TRIM7-deficient (KO) HaCaT cells were stimulated with *Lm* (MOI = 10) for indicated time periods. Afterward, the cells were lysed for immunoblot assays. LC3-II density was shown in the right panels. (h) Wild-type (WT) and TRIM7-deficient (KO) HaCaT cells were transfected with GFP-LC3 plasmid. At 24 h after transfection, the cells were infected with *Lm* (MOI = 10) or left uninfected for 4 h, and then subjected to confocal microscopy analysis. Scale bars: 10 μ m. LC3 puncta quantification was shown in the left panel. (i) HeLa-mCherry-LC3 cells were transfected with control siRNA (SC) or TRIM7-specific siRNA (R3). At 24 h after transfection, the cells were infected with *Lm* (MOI = 10) or left uninfected for 4 h, and then subjected to confocal microscopy analysis. Scale bars: 10 μ m. LC3 puncta quantification was shown in the bottom panel. (j) PMA-THP1 cells were transfected with control siRNA (SC) or TRIM7-specific siRNA (R3). At 24 h after transfection, the cells were infected with *Lm* (MOI = 10) for indicated time periods. Afterward, the cells were lysed for immunoblot assays. LC3-II density was shown in the right panel. The data are representative of three independent experiments and are presented as mean \pm SD. *, $p < 0.05$, **, $p < 0.01$, ****, $p < 0.0001$.

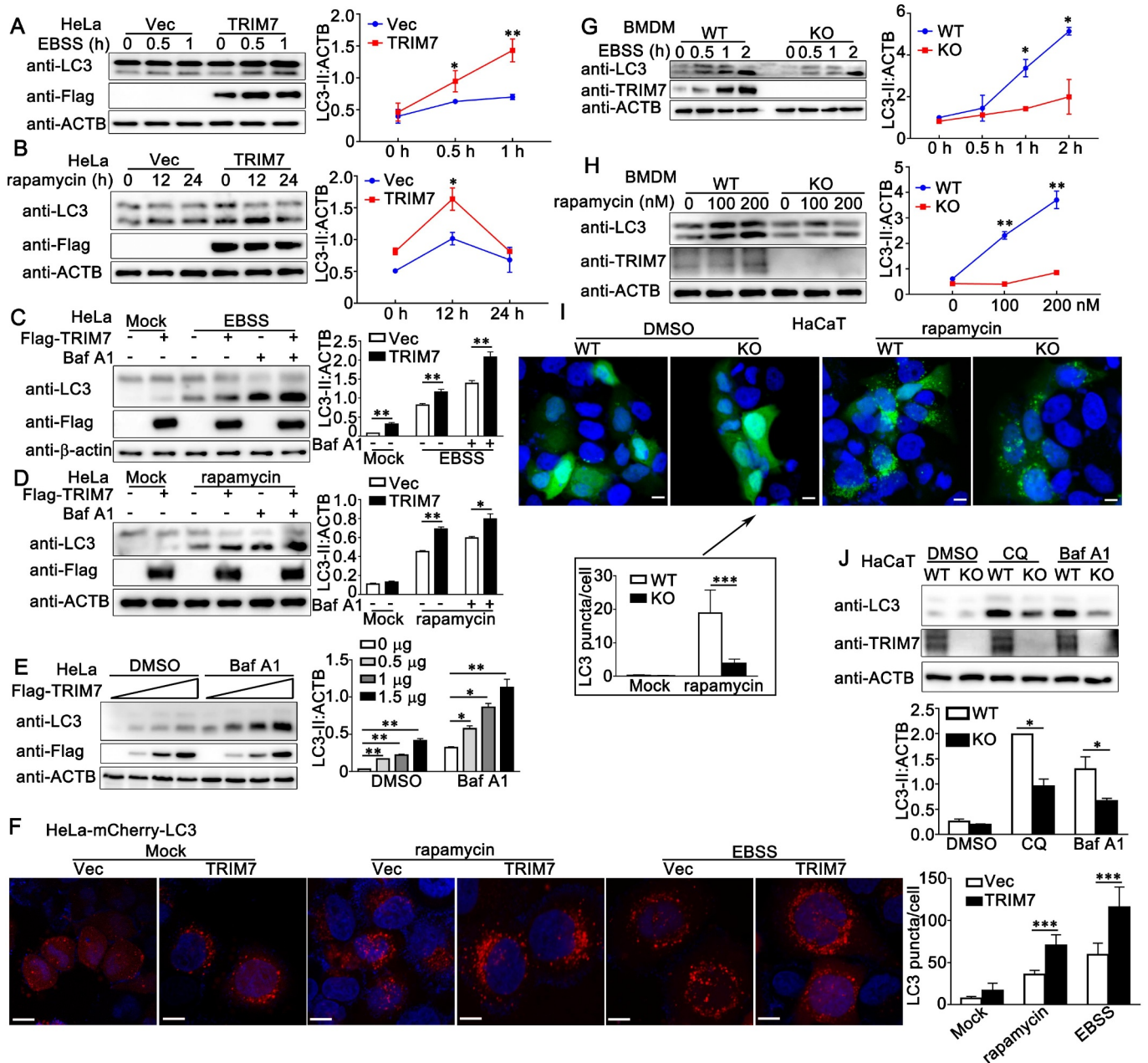


Figure 5. TRIM7 positively regulated autophagy. (A) HeLa cells were transfected with Vector (Vec) or Flag-TRIM7 and then treated with EBSS for indicated time periods. Afterward, the cell lysates were subjected to immunoblot analysis as indicated. LC3-II density was shown in the right panel. (B) HeLa cells were transfected with vector (Vec) or Flag-TRIM7. At 24 h after transfection, the cells were treated with rapamycin (200 nM) for indicated time periods. Afterward, the cells were lysed for immunoblot assays. LC3-II density was shown in the right panel. (C) HeLa cells were transfected with Vector (-) or Flag-TRIM7 (+) plasmids. At 24 h after transfection, the cells were treated with DMEM (with 10% FBS), EBSS, or EBSS with bafilomycin A₁ (Baf A1, 400 nM) for 2 h, and then subjected to immunoblot analysis. LC3-II density was shown in the right panel. (D) HeLa cells were transfected with Vector (-) or Flag-TRIM7 (+). At 24 h after transfection, the cells were treated with DMSO (Mock) or rapamycin (200 nM) for 12 h. Cells with rapamycin stimulation were treated with or without bafilomycin A₁ (Baf A1, 400 nM) for 2 h before collection. Then, the cells were subjected to immunoblot analysis. LC3-II density was shown in the right panel. (E) HeLa cells were transfected with different doses of Flag-TRIM7. At 24 h after transfection, the cells were treated with bafilomycin A₁ (Baf A1, 400 nM) or DMSO for 4 h, and then the cells were subjected to immunoblot analysis. LC3-II density was shown in the right panel. (F) HeLa-mCherry-LC3 cells were transfected with Vector (Vec) or TRIM7 plasmids. At 24 h after transfection, the cells were treated with rapamycin (200 nM) for 12 h, EBSS for 2 h, or DMEM with 10% FBS for 2 h, and then subjected to confocal microscopy analysis. Scale bars: 10 μm. LC3 puncta quantification was shown in the right panel. (G) Wild-type (WT) and *trim7*-deficient (KO) BMDMs were treated with EBSS for indicated time periods, and then the cells were lysed for immunoblot assays. LC3-II density was shown in the right panel. (H) Wild-type (WT) and *trim7*-deficient (KO) BMDMs were treated with different doses of rapamycin (0, 100, 200 nM) for 12 h. Afterward, the cells were lysed for immunoblot assays. LC3-II density was shown in the right panel. (I) Wild-type (WT) and *TRIM7*-deficient (KO) HaCaT cells, were transfected with GFP-LC3 (200 nM) or DMSO as a control for 12 h, and then subjected to confocal microscopy analysis. Scale bars: 10 μm. LC3 puncta quantification was shown in the bottom panel. (J) Wild-type (WT) and *TRIM7*-deficient (KO) HaCaT cells were treated with CQ (100 μM), bafilomycin A₁ (Baf A1, 400 nM) or DMSO as a control for 4 h, and then the cells were subjected to immunoblot analysis. LC3-II density was shown in the bottom panel. The data are representative of three independent experiments and are presented as mean ± SD. *, $p < 0.05$, **, $p < 0.01$, ***, $p < 0.001$.

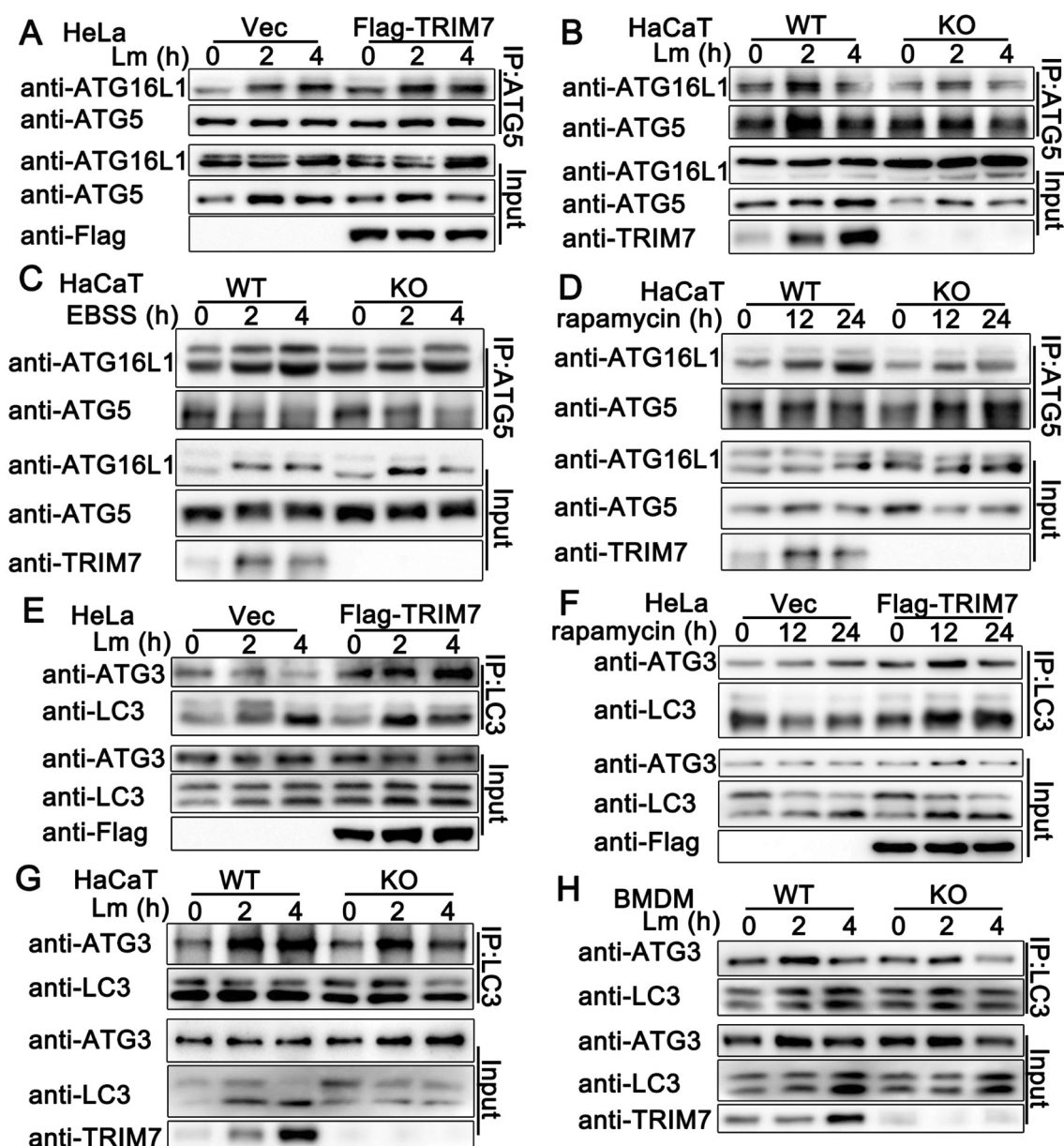


Figure 6. TRIM7 regulated ATG7-related ubiquitin-like conjugation systems in autophagy. (A) HeLa cells were transfected with Vector (Vec) or Flag-TRIM7, and then infected with *Lm* (MOI = 10) for indicated time periods. Afterward, the cell lysates were subjected to immunoprecipitation (IP) and immunoblot (IB) analysis as indicated. (B) Wild-type (WT) and *TRIM7*-deficient (KO) HaCaT cells were infected with *Lm* (MOI = 10) for indicated time periods. Afterward, the cell lysates were subjected to immunoprecipitation (IP) and immunoblot (IB) analysis as indicated. (C, D) Wild-type (WT) and *TRIM7*-deficient (KO) HaCaT cells were treated with EBSS (C) or rapamycin (D) for indicated time periods. Afterward, the cell lysates were subjected to immunoprecipitation (IP) and immunoblot (IB) analysis as indicated. (E) HeLa cells were transfected with Vector (Vec) or TRIM7-encoding plasmids, and were infected with *Lm* (MOI = 10) for indicated time periods. Afterward, the cell lysates were subjected to immunoprecipitation (IP) and immunoblot (IB) analysis as indicated. (F) HeLa cells were transfected with Vector (Vec) or Flag-TRIM7, and then treated with rapamycin for indicated time periods. Afterward, the cell lysates were subjected to immunoprecipitation (IP) and immunoblot (IB) analysis as indicated. (G, H) Wild-type (WT) and *TRIM7*-deficient (KO) HaCaT cells (G) or BMDMs (H) were infected with *Lm* (MOI = 10) for indicated time periods. Afterward, the cell lysates were subjected to immunoprecipitation (IP) and immunoblot (IB) analysis as indicated. The data are representative of three independent experiments.

polyubiquitin chains can be generated, among which K48- and K63-linked ubiquitination is the most studied types of linkage [31]. K48-linked ubiquitination usually mediates the degradation of protein in a proteasome-dependent way, whereas K63-linked modification mainly regulates signal transduction in a non-proteolytic manner [32]. To identify the type of linkage that was promoted by TRIM7, we used expression plasmids for ubiquitin mutants retaining only a single lysine residue. Immunoprecipitation and immunoblot analysis indicated that TRIM7 promoted only K63 mutants (only the Lys residue 63

was retained) mediated ubiquitination of ATG7, suggesting TRIM7 enhanced the K63-linked ubiquitination of ATG7 (Figure 7c). This phenomenon was further confirmed by the usage of K48R (only the Lys residue 48 was mutated to Arg) and K63R (only the Lys residue 63 was mutated to Arg). As shown in Figure 7d, TRIM7 increased K48R mediated ubiquitination of ATG7, but not K63R, indicating the Lys residue 63 was essential to the TRIM7-triggered linkage of ATG7 with ubiquitin (Figure 7d). Further, *in vitro* ubiquitination assays suggested that TRIM7 promoted the ubiquitination of ATG7

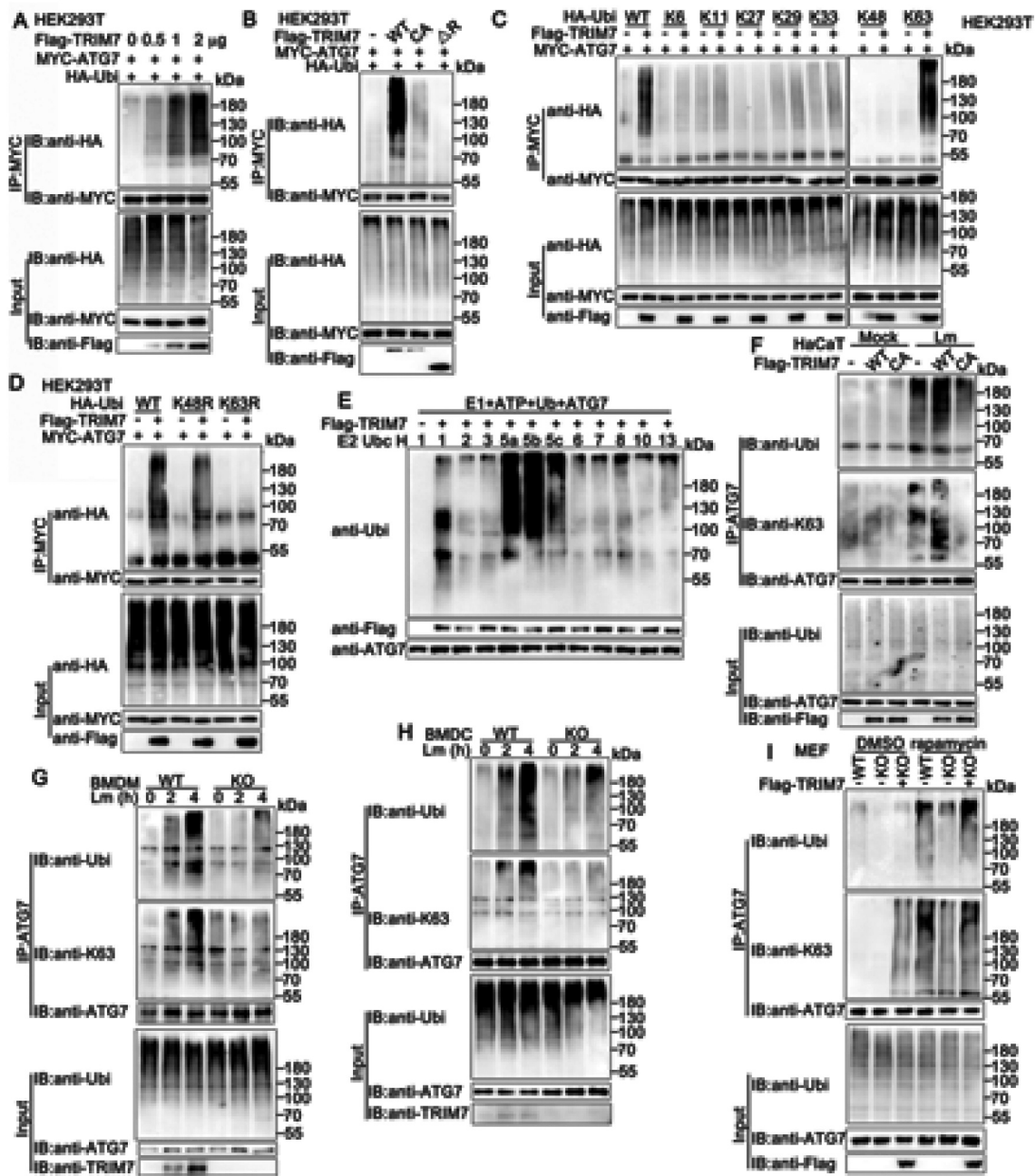


Figure 7. TRIM7 promoted the ubiquitination of ATG7. (A) HEK293T cells were transfected with Myc-ATG7, HA-Ubi, and increasing doses of Flag-TRIM7 (0, 0.5, 1, and 2 μ g). At 24 h after transfection, the cells were lysed and subjected to immunoprecipitation (IP) and immunoblot (IB) analysis. (B) HEK293T cells were transfected with the indicated plasmids. At 24 h after transfection, immunoprecipitation (IP) and immunoblot (IB) analysis were performed as indicated. CA, TRIM7^{C29, 32A} mutant; Δ R, 85–511aa of TRIM7. (C, D) HEK293T cells were transfected with plasmids as indicated. 24 h later, immunoprecipitation (IP) and immunoblot (IB) analysis were performed as indicated. (E) Immunoblot analysis of ATG7 ubiquitination *in vitro*. ATG7 and wild-type TRIM7 were quickly translated *in vitro*, and then, the biotin-ubiquitin E1 and indicated E2s were added for *in vitro* ubiquitination assays. Ubiquitination of ATG7 was detected by anti-Ubi. (F) Wild-type (WT) and TRIM7-deficient (KO) HaCaT cells, were transfected with plasmids as indicated and then infected with *Lm* for 4 h. Afterward, the cells were lysed for immunoprecipitation (IP) and immunoblot (IB) assays. CA, TRIM7^{C29, 32A} mutant. (G, H) Wild-type (WT) and *trim7*-deficient (KO) BMDMs (G) or BMDCs (H) were infected with *Lm* for indicated time periods. Afterward, the cells were lysed for immunoprecipitation (IP) and immunoblot (IB) assays. (I) Wild-type (WT) and *trim7*-deficient (KO) MEFs were transfected with Vector (-) or TRIM7 (+) plasmids, and were stimulated with rapamycin for 12 h. Afterward, the cell lysates were subjected to immunoprecipitation (IP) and immunoblot (IB) analysis as indicated. The data are representative of three independent experiments.

directly using UBC5 as a ubiquitin-conjugating E2 enzyme, but the C29,32A and Δ R mutants of TRIM7 did not (Figure 7e and S3b).

Next, we investigated the effects of TRIM7 on the ubiquitination of ATG7 during autophagy that was triggered by *L. monocytogenes* infection, starvation, or rapamycin. Firstly, we examined whether the ubiquitination of ATG7 was induced in

these conditions. As shown in Figure 7f and Figure S3c, upon the treatment of *L. monocytogenes* infection, starvation, or rapamycin, the ubiquitination of ATG7 was significantly induced. Then, the role of TRIM7 in the ubiquitination of ATG7 in these conditions was evaluated. Wild-type or *trim7*-deficient BMDMs, BMDCs, or MEFs were infected with *L. monocytogenes* and then subjected to the examination of ubiquitination of ATG7.

Immunoprecipitation and immunoblots assays indicated that *L. monocytogenes* infection induced the ubiquitination of ATG7 and the ubiquitination was impaired by *trim7*-deficiency (Figure 7g,h and S3d). Further, in MEFs, *trim7* deficiency decreased rapamycin-triggered ubiquitination of ATG7 and this decrease was rescued by TRIM7 transfection (Figure 7i). Meantime, upon the treatment of starvation or rapamycin, TRIM7 overexpression in HeLa cells increased the K63-linked ubiquitination of ATG7 (Figure S3E) whereas TRIM7 silence in PMA-THP1 cells inhibited it (Figure S3F). Taken together, these findings suggest TRIM7 promotes the K63-linked ubiquitination of ATG7 with the treatment of *L. monocytogenes* infection, starvation, or rapamycin.

E3 ligase activity of TRIM7 is critical to its role in the regulation of autophagy

Considering that TRIM7 regulated the ubiquitination of ATG7 as an E3 ligase and TRIM7 manipulated autophagy, we examined whether the E3 ligase activity of TRIM7 was essential to its role in autophagy. TRIM7 or its C29, 32A mutant were transfected into HeLa cells. After *L. monocytogenes* infection, LC3-II was detected by immunoblots and the results demonstrated that C29, 32A mutant, which lost the ability to increase the ubiquitination with the destroyed RING domain (Figure 7b), made little difference in LC3-II accumulation whereas wild-type TRIM7 promoted the accumulation of LC3-II (Figure 8a). Similar results were observed in HeLa cells with the treatment of starvation (Figure 8b). Further, to exclude the possible effects of endogenous TRIM7, TRIM7 or its mutants were transfected into *trim7*-deficient MEFs, followed by *L. monocytogenes* infection or rapamycin stimulation. As shown in Figure 8c, in *trim7*-deficient MEFs with *L. monocytogenes* infection, whereas TRIM7 transfection increased LC3-II accumulation, the C32, 29A, and the ΔR mutant of the TRIM7 barely affected LC3-II accumulation. Consistently, in response to the stimulation of rapamycin, C29, 32A mutant of TRIM7 did not significantly affect the accumulation of LC3-II as wild-type TRIM7 did (Figure 8d). In all, these results indicate that the E3 ligase activity of TRIM7 is essential to its regulation of autophagy.

TRIM7 promotes ubiquitination of ATG7 at K413

To investigate whether the ubiquitination of ATG7 by TRIM7 was essential to its function in autophagy, we explored the ubiquitination site at ATG7 that was targeted by TRIM7. Potential ubiquitination sites at ATG7 were predicted by CPLM4.0, a database for protein lysine modifications [33]. Then ATG7 mutants were constructed with these potential lysine sites replaced by arginine separately. As shown in Figure 9a, A series of ATG7 mutants were transfected into HEK293T cells, together with Myc-TRIM7 and HA-Ubi, and the ubiquitination of ATG7 was examined. Immunoprecipitation and immunoblot analysis indicated that the K413R mutant of ATG7 could not be ubiquitinated by TRIM7, suggesting TRIM7 promoted the ubiquitination of ATG7 at K413 (Figure 9a). Protein alignments revealed that the K413 was located in the E1-like domain of ATG7 and was highly conserved among species (Figure 9b). Next, we investigated

whether the mutation at K413 affected the function of ATG7. Wild-type, K413R or K423R (the mutant with the same level of ubiquitination by TRIM7 as wild-type ATG7) mutants of ATG7 were co-transfected with LC3 and immunoprecipitation and immunoblot analysis were performed. The results indicated that the ATG7-LC3 interaction was impaired by the mutation at K413, suggesting K413 was critical to the association of ATG7 with LC3 (Figure 9c). This phenomenon was confirmed by the impairment in the interaction of K413R with endogenous LC3 in *L. monocytogenes*-infected HeLa cells (Figure 9d). Next, we examined the effect of the K413 mutation on autophagy and *L. monocytogenes* infection. In HEK293T cells, with inhibition of lysosome activity by Baf A1, ATG7 overexpression resulted in elevated autophagosome accumulation, whereas the K413R mutant ATG7 barely affected LC-II protein accumulation (Figure 9e). Similar results were observed in *L. monocytogenes* infection-induced LC-II protein accumulation in HeLa cells (Figure 9f). In addition, ATG7 transfection in MEFs inhibited *L. monocytogenes* infection and the K413R mutant could not inhibit *L. monocytogenes* infection as much as the wild-type ATG7 did (Figure S4). Finally, given that the K413 of ATG7 is conserved among species and is located at K409 in mice (Figure 9b), we investigated the effect of the K409R mutant of mouse ATG7 on *L. monocytogenes* infection and autophagy in MEFs. As expected, the K409R mutant of mouse ATG7 could not inhibit *L. monocytogenes* infection to the same extent as the wild-type mouse ATG7 did (Figure 9g). However, in *trim7*-deficient MEFs, wild-type and K409R mutant of mouse ATG7 did not show a significant difference in their effect on *L. monocytogenes* infection, suggesting the modification on K409 by TRIM7 played an important role in the function of ATG7 (Figure 9g). Consistent with the results from K413R, the ATG7-promoted autophagosome accumulation was impaired by the mutation at K409 in MEFs (Figure 9h). It has been reported that the Phe403Leu (F403L) variant of ATG7 impairs autophagy and is detected in patients with primary ovarian insufficiency/POI, but the underlying mechanism by which the F403L mutant impaired the role of ATG7 in autophagy is unclear [34,35]. Considering that the site of F403 is very close to K413, both of which are in the E1-like domain of ATG7, we examined whether the mutation at the site of 403 affected the association of ATG7 with TRIM7 and its ubiquitination. Our findings demonstrated that compared to wild-type ATG7, the F403L mutant exhibited decreased ubiquitination and weaker interaction with TRIM7, suggesting TRIM7 might contribute to the impairment of autophagy by the F403L mutant of ATG7 (Figure 9i,j). In all, our findings demonstrate that TRIM7 promotes the ubiquitination of ATG7 at K413, and ubiquitination at this site is critical to the function of ATG7 in autophagy and *L. monocytogenes* infection.

Discussion:

Based on our previous work, TRIM7 plays an important role in the anti-viral innate immune responses via two different mechanisms [25,26]. TRIM7 negatively regulates DNA virus or RNA virus-triggered innate immune responses targeting STING1 or MAVS separately, by promoting the K48-linked ubiquitination and subsequent proteasome-dependent degradation of target proteins [25,26]. Given the similarities between the innate responses to

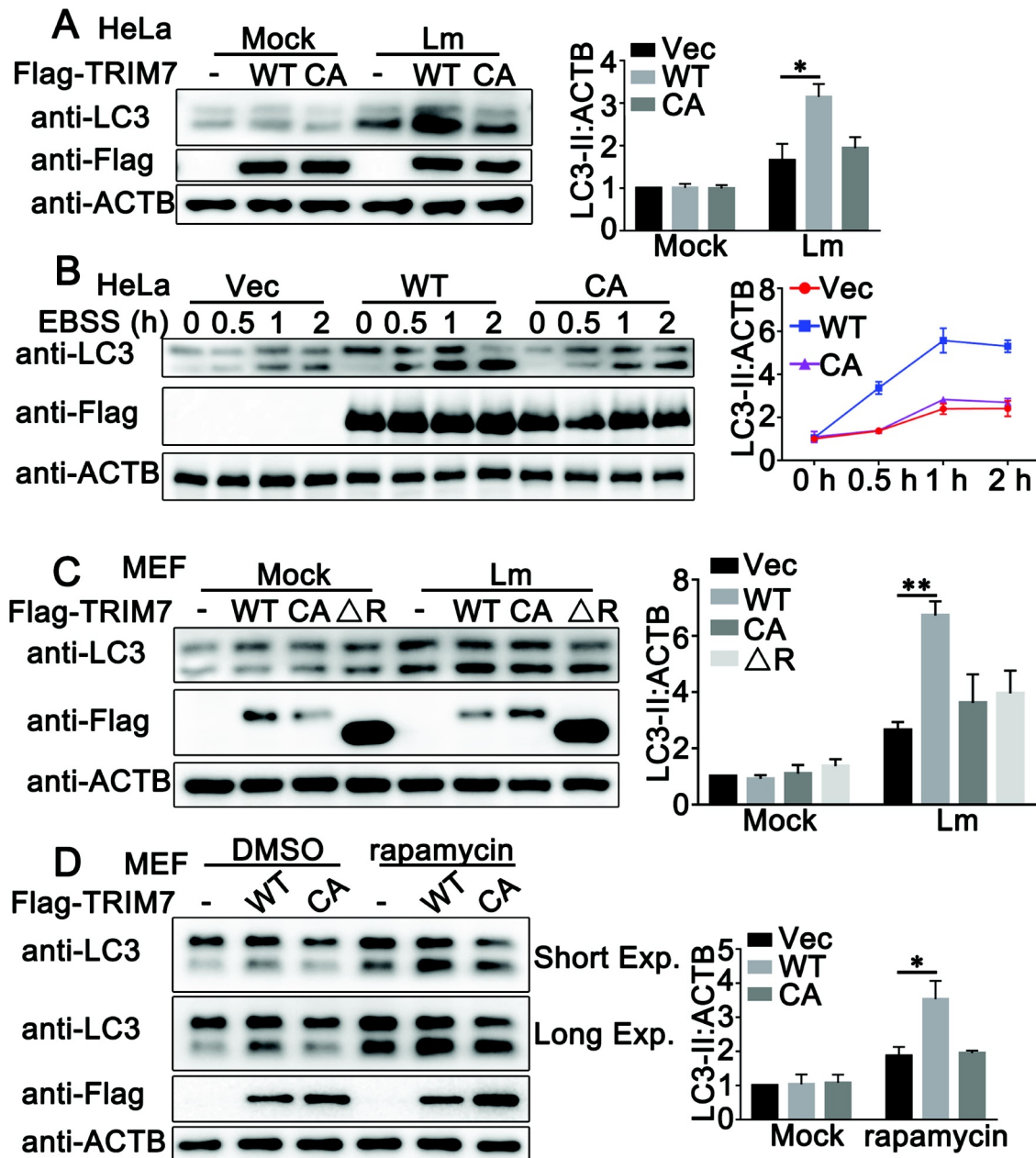


Figure 8. Ubiquitination is critical to the effect of TRIM7 on autophagy. (A) HeLa cells, were transfected with Vector (-), wild-type TRIM7 (WT) or C29, 32A mutant (CA), and then infected with *Lm* (MOI = 10) for 2 h. Afterward, the cells were lysed for immunoblot assays. LC3-II density was shown in the right panel. (B) HeLa cells were transfected with Vector (Vec), wild-type TRIM7 (WT) or C29, 32A mutant (CA), and then treated with EBSS for indicated time periods. Afterward, the cells were lysed for immunoblot assays. LC3-II density was shown in the right panel. (C) *trim7*-deficient (KO) MEFs, were transfected with Vector (-), wild-type TRIM7 (WT), C29, 32A mutant (CA) or 85–511aa of TRIM7 (ΔR), and then infected with *Lm* or left uninfected for 2 h. Afterward, the cells were lysed for immunoblot assays. LC3-II density was shown in the right panel. (D) *trim7*-deficient (KO) MEFs, were transfected with Vector (-), wild-type TRIM7 (WT) or C29, 32A mutant (CA), and then treated with DMSO or rapamycin (200 nM) for 12 h. LC3-II density was shown in the right panel. The data are representative of three independent experiments and are presented as mean \pm SD. *, $p < 0.05$, **, $p < 0.01$.

viruses and intracellular bacteria, these findings about TRIM7 prompted us to explore the role of TRIM7 in intracellular bacterial infection, using *L. monocytogenes* as a model. Consistent with the results from virus infection, TRIM7 deficiency in mice resulted in elevated IFN β production upon *L. monocytogenes* infection. Surprisingly, with higher IFN β expression levels than wild-type mice, TRIM7-deficient mice exhibited a lower survival rate and an increase in *L. monocytogenes* infection following *L. monocytogenes* infection. Confused with these findings in mice, we further examined the role of TRIM7 in *L. monocytogenes* infection at the cellular

level. Consistent with the results from *trim7*-deficient mice, TRIM7 knockdown in PMA-THP1 cells or *trim7* deficiency in BMMs, BMDCs, MEFs, PMs, or HaCaT cells promoted both *L. monocytogenes* infection and *L. monocytogenes* triggered innate immune responses, including the production of IFN β , CXCL10, IFIT1 and TNF and the phosphorylation of TBK1, IRF3, and RELA. Given that STING1 is required for the type I IFN response to *L. monocytogenes* infection [36], to exclude the regulatory effects of TRIM7 on STING1, we further tested the role of TRIM7 on *L. monocytogenes* infection in STING1-deficient THP1 cells and

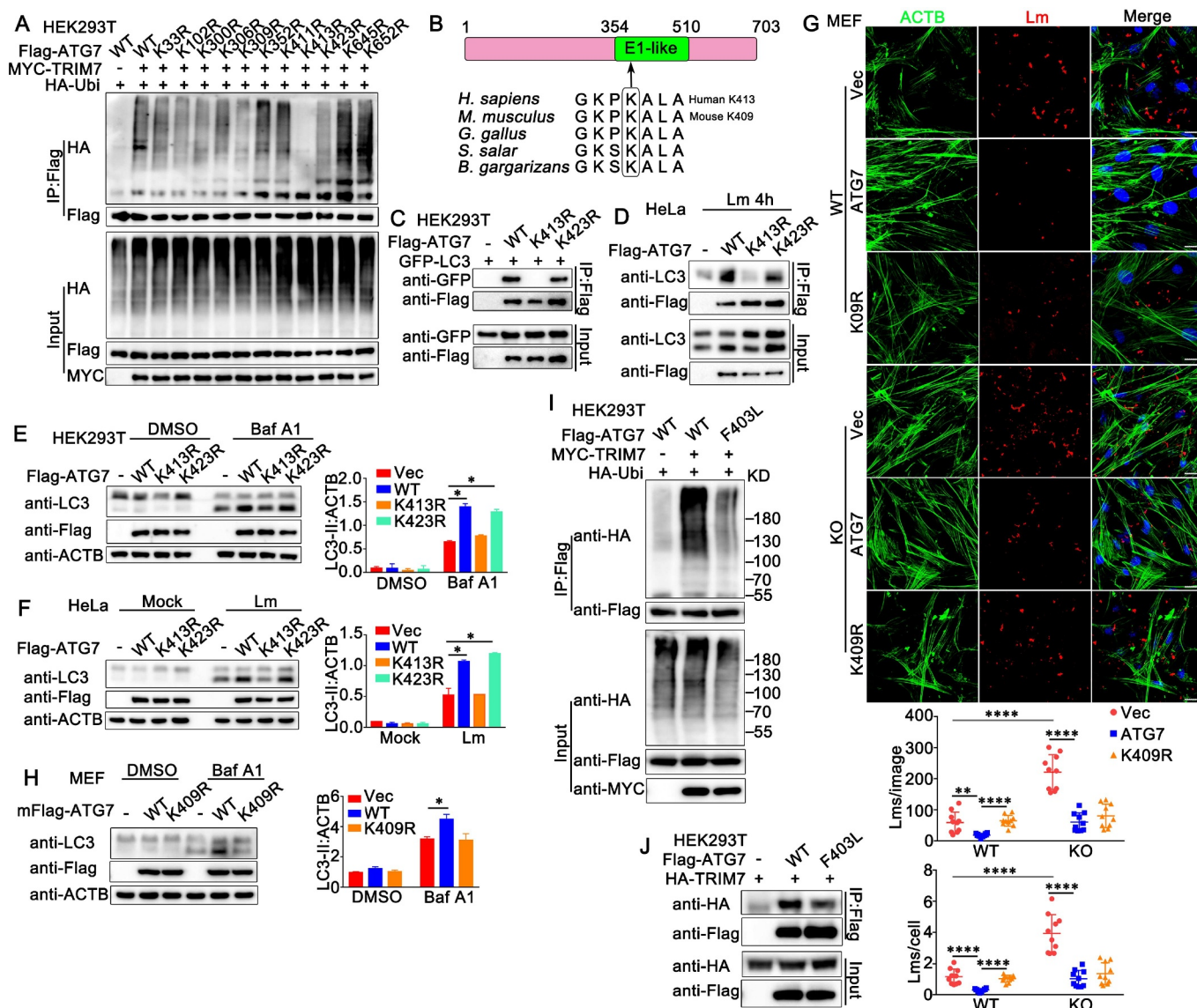


Figure 9. TRIM7 targeted ATG7 for K63-mediated ubiquitination at K413. (A) HEK293T cells were transfected with the indicated plasmids. At 24 h after transfection, immunoprecipitation (IP) and immunoblot (IB) analysis were performed as indicated. (B) Schematic representation of ATG7 protein and interspecific sequence alignments of genomic regions carrying the interchanged amino acids. E1-like domain, E1 activating enzyme-like. (C) HEK293T cells were transfected with the indicated plasmids. At 24 h after transfection, immunoprecipitation (IP) and immunoblot (IB) analysis were performed as indicated. (D) HeLa cells were transfected with indicated plasmids, and then stimulated with *Lm* (MOI = 10) for 4 h. Afterward, the cells were lysed and subjected to immunoprecipitation (IP) and immunoblot analysis as indicated. (E) HEK293T cells, were transfected with Flag-tagged ATG7 or its mutants as indicated, and then treated with Baf A1 (400 nM) or DMSO as a control for 4 h. The cells were subjected to immunoblot analysis. LC3-II density was shown in the right panel. (F) HeLa cells were transfected with indicated plasmids, and then stimulated with *Lm*, (MOI = 10) for 4 h. Afterward, the cells were lysed for immunoblot analysis. LC3-II density was shown in the right panel. (G) Wild-type (WT) or *trim7*-deficient (KO) MEFs were transfected with Flag-tagged mouse ATG7 or its mutant mK409R. 24 h later, the cells were infected with *Lm* or left uninfected for another 6 h, and then subjected to confocal analysis. The top panel shows DAPI (blue), *Lm* (red), ACTB (green), and merged views of three channels. Scale bars: 20 μ m. The bottom panel shows the statistical analysis of the total number of bacteria and the number of bacteria per cell in all pictures (10 pictures per genotype). (H) Wild-type MEFs were transfected with Flag-tagged mouse ATG7 or its mutant and then treated with Baf A1 (400 nM) or DMSO as a control for 4 h. The cells were subjected to immunoblot analysis. LC3-II density was shown in the right panel. (I) HEK293T cells were transfected with indicated plasmids, and then the cell lysates were subjected to immunoprecipitation (IP) and immunoblot. (IB) analysis as indicated. (J) HEK293T cells were transfected with indicated plasmids, and then the cell lysates were subjected to immunoprecipitation (IP) and immunoblot. The data are representative of three independent experiments and are presented as mean \pm SD. *, $p < 0.05$, **, $p < 0.01$, ****, $p < 0.0001$.

the results demonstrated that TRIM7 could negatively regulate *L. monocytogenes* infection in a STING1-independent way. These *in vivo* and *in vitro* observations indicated that TRIM7 might manipulate *L. monocytogenes* infection through some mechanism other than the regulation of innate signaling pathways.

Considering that TRIM7 is an E3-ligase, to explore the underlying mechanism by which TRIM7 regulated

L. monocytogenes infection, we first tried to identify the potential substrate of TRIM7. Comparing the proteins that were immunoprecipitated with or without TRIM7, a few TRIM7-associated proteins were identified by mass spectrum. Among these proteins, ATG7, which is a well-known essential protein to autophagy, was found at the top of the protein "hit list". Central to canonical autophagy are two ubiquitination-

like conjugation systems, the ATG12 conjugation system, and the LC3/ATG8 lipidation system, both of which are activated by the same E1-like enzyme, ATG7 [37]. With ATG7 as an E1-like enzyme and ATG10 as an E2-like enzyme, ATG12 is attached to ATG5 [38]. Then the ATG12–ATG5–ATG16L1 complex assists the conjugation of LC3 to PE, catalyzed by ATG7 and ATG3 as E1-like and E2-like enzymes respectively [39]. Therefore, the association of TRIM7 with ATG7 provided us hint that TRIM7 might be involved in the regulation of autophagy.

It has become clear that autophagy is a major mechanism by which the host cells eliminate invading pathogens, including viruses and intracellular bacteria [39]. In addition to host cell recognition of *L. monocytogenes* PAMPs by DNA sensors or NLRs, *L. monocytogenes* and its secreted toxin, LLO, can be targeted by the Ub-SQSTM1/p62-LC3 pathway to autophagy [4,36]. The deficiency in autophagy genes, such as *Atg5* and *Atg7*, increases susceptibility to intracellular bacteria, including *Mycobacterium (M) tuberculosis* and *L. monocytogenes* [40–43]. Thus, after the confirmation of the TRIM7-ATG7 interaction, we examined the effects of TRIM7 on *L. monocytogenes* infection-triggered autophagy by the over-expression, knockdown, or deficiency of TRIM7 in a variety range of cells, including HeLa, BMDMs, BMDCs, PMs, and HaCaT cells. Both the level of LC3-II in immunoblot assays and the amounts of LC3-II puncta by confocal microscopy suggest a positive regulatory role of TRIM7 in *L. monocytogenes*-induced autophagy. Further, the treatment with bafilomycin A₁, an inhibitor of vascular proton pump that indirectly blocks the fusion of autophagosomes to lysosomes, and with chloroquine, the lysosome acidification inhibitors, indicated that TRIM7 promoted *L. monocytogenes*-induced autophagosome accumulation, but not the phagosome-lysosome fusion or lysosomal degradation. In addition to the role in *L. monocytogenes*-induced autophagy, our findings demonstrated that TRIM7 also positively manipulated basal, and starvation- or rapamycin-activated autophagy.

Given that ATG7 is critical to canonical autophagy, modifications of ATG7 may be an efficient way to regulate autophagic response under a variety of conditions. However, till now, few posttranslational modifications have been identified to manipulate autophagy targeting ATG7. Our previous study has revealed that the beta chain of the non-classical MHC-II protein HLA-DM interacts with ATG7 and increases its acetylation, leading to reduced autophagosome accumulation and human T-cell leukemia virus type-1/HTLV-1 infection [44]. Recently, NEDD4 was identified to promote the ubiquitination and subsequent degradation of ATG7 [38]. In this study, we demonstrated that the K63-linked ubiquitination of ATG7 was induced by a variety range of conditions, including starvation, rapamycin stimulation, and *L. monocytogenes* infection. This ubiquitination could be significantly promoted by ATG7 and the RING domain of TRIM7 was required for the ubiquitination of ATG7. The examination of the association of the ATG5-ATG16L1 and ATG3-LC3 indicated that TRIM7 regulated ATG7-involved ubiquitination-like conjugation systems in autophagy. Further, the C29, 32A, and ΔR mutants of TRIM7 lacking the ability of ubiquitination lost their effects

on the regulation of autophagosome accumulation. Finally, we identified the ubiquitination site at ATG7 that was catalyzed by TRIM7. K413R mutant of ATG7 lost not only the ubiquitinated modification by TRIM7 but also the capability to promote autophagy, leading to less efficient inhibition of *L. monocytogenes* infection compared to wild-type ATG7. These findings indicated that the ubiquitination of ATG7 at K413 by TRIM7 was required for the function of ATG7 in autophagy and *L. monocytogenes* infection. Further, the reported F403L variant in primary ovarian insufficiency patients as a loss of function mutant of ATG7 was found to have impairment in ubiquitination and interaction with TRIM7, suggesting an essential role of TRIM7-mediated ubiquitination in autophagy.

A few limitations should be noted. In this study, we screened TRIM7-associated proteins in unstimulated HEK293T cells, therefore some other proteins might be overlooked. In addition, future screening for immune or epithelial cells' response upon *L. monocytogenes* infection, may further expand our understanding of the role of TRIM7 in *L. monocytogenes* infection in different tissues. Notably, the fact that the ubiquitination of ATG7 could be detected in TRIM7-deficient cells, suggests that other E3 ligases responsible for ATG7 ubiquitination may exist. Thus, screening for additional ATG7-associated E3 ligases, may shed more light on the modification of ATG7.

Together, our study demonstrated that TRIM7 positively regulated autophagosome accumulation by promoting the ubiquitination of ATG7 at K413, thereby affecting *L. monocytogenes* infection (Figure 10). Our findings suggested a new regulator in intracellular bacterial infection and autophagy, with a novel posttranslational modification that targeted ATG7 at K413. This research may expand our understanding of host anti-bacterial defense and the role of autophagy in intracellular bacterial infection.

Materials and methods

Mice

We generated *trim7*-deficient mice as described previously [26]. Mice were housed in a facility with access to food and water and were maintained under a 12-h light/12-h dark cycle. All animal procedures were performed according to guidelines approved by the committee on animal care at Xixiang Medical University, China. The age- and sex-matched wild-type and *trim7*-deficient mice were used in the experiments.

cDNA constructs and reagents

Human *ATG7* or mouse *Atg7* were amplified by PCR using cDNA from THP1 or MEF cells and were subsequently cloned into a pcDNA3 vector (Invitrogen, V79520). *ATG7* mutants were constructed by PCR and also subcloned into a pcDNA3 vector. Human *TRIM7* and its mutants were generated as described previously [26]. GFP-LC3, HA-Ubi, HA-K6-Ubi, HA-K11-Ubi, HA-K27-Ubi, HA-K29-Ubi, HA-K33-Ubi, HA-K48-Ubi, HA-K63-Ubi, HA-K48R-Ubi, and HA-K63R-Ubi

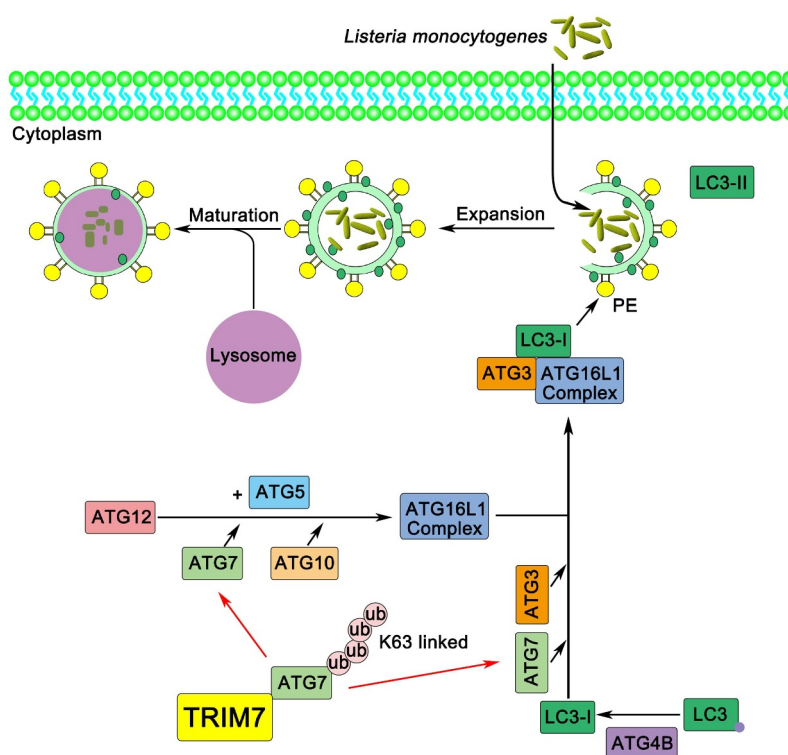


Figure 10. Working model of the mechanism by which TRIM7 regulates autophagy. In this model, TRIM7 enhances K63-linked poly-ubiquitination of ATG7, which in turn promotes autophagy, thereby increasing the clearance of *L. monocytogenes*.

were obtained as described previously [44–46]. The following antibodies were used for immunoblot analysis or immunoprecipitation: anti-Flag (Sigma-Aldrich, 3165), anti-HA (Biolend, 901,515), anti-MYC (Proteintech, 66,004-1-Ig), anti-TRIM7/RNF90 (Santa Cruz Biotechnology, sc-109,107; Abcam, ab170538), anti-ATG7 (Cell Signaling Technology, 8588), anti-p-TBK1 (Cell Signaling Technology, 5483 T), anti-TBK1 (Flarbio, CSB-PA024154LA01HU), anti-p-IRF3 (Cell Signaling Technology, 4947), anti-IRF3 (Proteintech, 11,312-1-AP), anti-p-RELA/p65 (Cell Signaling Technology, 3033), anti-RELA/p65 (Proteintech, 10,745-1-AP), anti-Ubi (Santa Cruz Biotechnology, sc-8017), anti-Ubi-K63 (Millipore, 05-1313), anti-LC3 (Proteintech, 14,600-1-AP; MBL, PM036), anti-ATG3 (Cell Signaling Technology, 3415), anti-ATG5 (Cell Signaling Technology, 12,994), anti-ATG16L1 (8089, Cell Signaling Technology), anti-*Lm* (Abcam, ab35132), and anti-ACTB/ β -actin (Proteintech, 60,008-1). The PMA (S1819) and rapamycin (S1842) were purchased from Beyotime Biotechnology. Bafilomycin A₁ (11,038) was obtained from Cayman Chemical. Chloroquine (C6628) was purchased from Sigma-Aldrich.

Cell culture, transfection, and stimulation

Human embryonic kidney (HEK) 293 T and Tohoku Hospital Pediatrics (THP) 1 cells were kindly provided by Stem Cell Bank, Chinese Academy of Sciences. HaCaT keratinocytes were purchased from Procell Life Science & Technology Co., Ltd., (CL-0090). HeLa-mCherry-LC3 cells were kindly provided by Yuna Niu (Xinxiang Medical University). STING1-

deficient THP1 cells were purchased from InvivoGen (thpd-kostg). HaCaT and HEK293T cells were cultured in Dulbecco's modified Eagle's medium (DMEM; Sigma-Aldrich, D6429). THP1 cells were grown in RPMI 1640 (Gibco, C22400500BT). PMA-THP1 cells referred to THP1 cells that were pretreated with 100 ng/ml PMA for 24 h. All cells were supplemented with 10% FBS (Gibco, 10,099-141), 4 mM L-glutamine, 100 μ g/ml penicillin, and 100 U/ml streptomycin under humidified conditions with 5% CO₂ at 37°C. Transfection of HaCaT, HEK293T, THP1, MEF, and BMDM cells was performed with Lipofectamine 2000 (Invitrogen, 11,668-019) according to the manufacturer's instructions.

Preparations of BMDMs, BMDCs, peritoneal macrophages and MEFs

The procedure for generating BMDMs, BMDCs, and MEFs has been described previously [25,47,48]. For the generation of peritoneal macrophages (PMs), wild-type and TRIM7-deficient mice were injected intraperitoneally with 2.5 mL of a 4% Brewers TG solution (Sigma-Aldrich, 70,157). After 4 days, when most recruited cells were macrophages, mice were killed and peritoneal cells were collected by lavage with 5 mL complete RPMI 1640 media. The lavage fluid was centrifuged, then the supernatant was aspirated, and the cell pellet was resuspended in a complete medium. Macrophages were further purified by adherence for 3 to 4-h at 37°C, at which point all nonadherent (nonmacrophage) cells were eliminated. Cells were maintained in RPMI 1640 media.

Immunoprecipitation and immunoblot analysis

Immunoprecipitation and immunoblot analysis were performed as described previously [49,50]. In short, after the treatment, the cells were lysed in lysis buffer containing 1.0% (vol:vol) Nonidet P40 (Solarbio, N8030), 20 mM Tris-HCl, pH 8.0, 10% (vol:vol) glycerol, 150 mM NaCl, 0.2 mM Na_3VO_4 , 1 mM NaF, 0.1 mM sodium pyrophosphate and a protease inhibitor “cocktail” (Roche, 04693132001). After centrifugation for 20 min at 14,000 g, supernatants were collected and incubated with the indicated antibodies together with protein A/G Plus-agarose immunoprecipitation reagent (Sc-2003, Santa Cruz Biotechnology) at 4°C for 3 h or overnight. After three washes, the immunoprecipitates were boiled in SDS sample buffer for 10 min and analyzed by immunoblot.

Real-time PCR

Total RNA was extracted from the cultured cells with TRIzol reagent (Invitrogen, 15,596,026) as described by the manufacturer. All gene transcripts were quantified by real-time PCR with SYBR Green qPCR Master Mix (Vazyme, Q711-02) using a 7500 Fast real-time PCR system (Applied Biosystems). The relative fold induction was calculated using the $2^{-\Delta\Delta\text{Ct}}$ method. The primers used for real-time PCR were as follows:

Human *IFNB*,

Forward, 5'-CACGACAGCTCTTTCCATGA-3';

Reverse, 5'-AGCCAGTGCTCGATGAATCT-3'

Human *CXCL10*,

Forward, 5'-GGTGAGAAGAGATGTCTGAATCC-3';

Reverse, 5'-GTCCATCCTTGGAAGCACTGCA-3'

Human *TNF*,

Forward, 5'-GGCGTGGAGCTGAGAGATAAC-3';

Reverse, 5'-GGTGTGGGTGAGGAGCACAT-3'

Human *IFIT1*,

Forward, 5'-GCCATTTTCTTTGCTTCCCCTA-3';

Reverse, 5'-TGCCCTTTTGTAGCCTCCTTG-3'

Human *GAPDH*,

Forward, 5'-TCAACGACCACTTTGTCAAGCTCA-3';

Reverse, 5'-GCTGGTGGTCCAGGTCTTACT-3'

Mouse *Ifnb*,

Forward, 5'-TCCTGCTGTGCTTCTCCACCACA-3';

Reverse, 5'-AAGTCCGCCCTGTAGGTGAGGTT-3'

Mouse *Cxcl10*,

Forward, 5'-ATCATCCCTGCGAGCCTATCCT-3';

Reverse, 5'-GACCTTTTTTGGCTAAACGCTTTC-3'

Mouse *Ifit1*,

Forward, 5'-TACAGGCTGGAGTGTGCTGAGA-3';

Reverse, 5'-CTCCACTTTCAGAGCCTTCGCA-3'

Mouse *Tnf*,

Forward, 5'-TCTTCTCATTCCTGCTTGTGG-3';

Reverse, 5'-GGTCTGGGCCATAGAAGTGA-3'

Mouse *Gapdh*,

Forward, 5'-ACGGCCGCATCTTCTTGTGCA-3';

Reverse, 5'-ACGGCCAAATCCGTTTACACC-3'.

ELISA

HaCaT cells were infected with *L. monocytogenes* for 24 h. The culture media were collected for measurement of IFNB (Proteintech, KE00044). Eight-week-old wild-type and *trim7*-deficient mice were intravenously infected with *L. monocytogenes* for 6 h, and then the serum of mice was collected for measurement of IFNB by ELISA.

RNA interference

TRIM7 knockdown experiments were performed as described previously [26]. *TRIM7* Stealth-RNAi siRNA was designed by the Invitrogen BLOCKiT RNAi Designer. The small interfering RNA (siRNA) sequences used were as follows: R3,

Forward, 5'-CAGUCUCUUCUGAGAUGAAGAAUAA-3';

Reverse, 5'-UUAUUCUUCUUCUCAGAAGAGACUG-3'

The Silencer Select negative control siRNA was purchased from Invitrogen (4,390,843). PMA-THP1, or HaCaT cells were transfected with siRNA using Lipofectamine 2000 according to the manufacturer's instructions. At 24 h after transfection, the cells were used for further experiments.

Generation of TRIM7 knockout cell line

TRIM7-deficient HaCaT cell line was generated by the CRISPR-Cas9 system as described previously [26]. The following oligonucleotides specifically targeting the *TRIM7* gene were used:

Oligonucleotide 1, 5'-

CACCGCTCACCTTGGATCCCGACA-3';

Oligonucleotide 2, 5'-

AAACTGTCTGGGATCCAAGGTGAGC-3'.

L. monocytogenes infections and enumeration of bacterial load

L. monocytogenes (*Lm*, 10403s) were kindly provided by Professor Yunwei Lou, Xinxiang Medical University. Bacteria were prepared by shaking in brain heart infusion (BHI) broth (OXOID, CM1135) with 50 µg/ml streptomycin overnight at 37°C. For infections, *L. monocytogenes* were grown to the mid-log phase and then resuspended in PBS (Solarbio, P1020). Age and sex-matched mice (6–10 weeks of age) were intravenously infected with *L. monocytogenes* (1.5×10^5 CFUs/mouse) and killed at day 3. To assess bacterial number in organs, lungs, livers, and spleens were homogenized and bacterial load was determined by serial dilution on BHI agar plates. For survival experiments, wild-type (WT) and *trim7*-deficient (KO) mice were intravenously infected with *L. monocytogenes* (1.5×10^5 CFUs/mouse). Mouse survival rates were monitored twice a day during 15 days of infection. BMDC, BMDMs, and HaCaT Cells were infected with *L. monocytogenes* at a multiplicity of infection (MOI) of 10 for 30 min at 37°C. To determine the number of bacteria entering the cells, extracellular bacteria were killed by treatment with 100 µg/ml gentamicin (Sigma-Aldrich, 1045–41-0) for an additional 30 min at 37°C. Then, infected cells were washed with PBS three times and lysed with 0.05% Triton

X-100 (Sigma-Aldrich, 9036–19-5) in distilled water. Serial dilutions were seeded on BHI agar plates and CFUs were counted after 36 h.

In vitro ubiquitination assay

ATG7, TRIM7, and its mutants were expressed with a TNT Quick-coupled Transcription/Translation Systems kit (Promega, L1171). *In vitro* ubiquitination assay was performed with a ubiquitination kit (Enzo Life Science, BML-UW9920) following the manufacturer's instructions.

Confocal microscopy

After treatment, HEK293T, MEFs, HeLa, and HaCaT cells were fixed with 4% PFA in PBS, permeabilized with Triton X-100, and then blocked with 1% BSA (Solarbio, A8020) in PBS. Nuclei were stained with 4, 6-diamidino-2-phenylindole (DAPI; Solarbio, C0065). ACTB was labeled with a phalloidin conjugate (ThermoFisher, A22287). Images were taken using Nikon A1R microscopy.

In situ PLA

MEFs were seeded on Thermanox plastic coverslips (NUNC, 174,950) and cultured overnight. After *L. monocytogenes* infection for 4 h, cells were fixed in 4% PFA in PBS for 15 min and washed with PBS three times. After that, cells were permeabilized with 0.1% Triton X-100 on ice for 5 min, washed in PBS and blocked in 5% BSA in PBS for 1 h at 37°C, and incubated in primary antibodies overnight at 4°C. On the next day, cells were washed with the wash buffer (Sigma-Aldrich, DUO82049) three times and incubated with the secondary antibodies with PLA probes (Sigma-Aldrich, DUO92001, DUO92005) for 2 h at 37°C followed by three times wash with the wash buffer. Cells were incubated with the Duolink *in situ* detection reagents red (Sigma-Aldrich, DUO92008) for 2 h at 37°C. Finally, Nuclei were stained with DAPI and covered onto slides. Images were taken using Nikon A1R microscopy and the Image Pro Plus 6.0 was used for quantitative analyses.

Mass spectrometry

Ten million HEK293T cells were seeded in a T75 flask overnight, and then the cells were transfected with Flag-TRIM7 plasmids for 24 h. Cell lysates were subjected to immunoprecipitation with anti-Flag and agarose beads at 4°C overnight. Proteins were separated by SDS-PAGE gel. After Coomassie Brilliant Blue staining, the gel bands of interest were excised from the gel and analyzed by liquid chromatography-mass spectrometry, which was performed by Applied Protein Technology Company.

Statistics

The data are presented as the means \pm SD from at least three independent experiments. The statistical comparisons between

the different treatments were performed using the Student t-test, and $p < 0.05$ was considered statistically significant.

Acknowledgments

We want to thank Dr. Yinming Liang for providing *trim7*-deficient mice and all the members of Henan Key Laboratory of immunology and targeted drugs for sharing valuable material and research support.

Disclosure statement

No potential conflict of interest was reported by the author(s).

Funding

This work was supported by the National Natural Science Foundation of China Grants (U1704183, 31970847, 32070949, U2004103, and 32170871); Natural Science Foundation of Henan Province (212300410065, 222300420064) Hainan Provincial Natural Science Foundation of China and Program for Science & Technology Innovation Talents in Higher Education of Henan Province (23HASTIT050) Higher Education of Henan province.

References

- [1] Galluzzi L, Baehrecke EH, Ballabio A, et al. Molecular definitions of autophagy and related processes. *EMBO J.* 2017;36(13):1811–1836.
- [2] Hansen M, Rubinsztein DC, Walker DW. Autophagy as a promoter of longevity: insights from model organisms. *Nat Rev Mol Cell Biol.* 2018;19(9):579–593.
- [3] Boya P, Reggiori F, Codogno P. Emerging regulation and functions of autophagy. *Nat Cell Biol.* 2013;15(7):713–720.
- [4] Ogawa M, Yoshikawa Y, Mimuro H, et al. Autophagy targeting of *Listeria monocytogenes* and the bacterial countermeasure. *Autophagy.* 2011;7(3):310–314.
- [5] Hamon M, Bierne H, Cossart P. *Listeria monocytogenes*: a multifaceted model. *Nat Rev Microbiol.* 2006;4(6):423–434.
- [6] Birmingham CL, Higgins DE, Brumell JH. Avoiding death by autophagy: interactions of *Listeria monocytogenes* with the macrophage autophagy system. *Autophagy.* 2008;4(3):368–371.
- [7] Py BF, Lipinski MM, Yuan J. Autophagy limits *Listeria monocytogenes* intracellular growth in the early phase of primary infection. *Autophagy.* 2007;3(2):117–125.
- [8] Zhao Z, Fux B, Goodwin M, et al. Autophagosome-independent essential function for the autophagy protein Atg5 in cellular immunity to intracellular pathogens. *Cell Host Microbe.* 2008;4(5):458–469.
- [9] Mizushima N, Yoshimori T, Ohsumi Y. The role of Atg proteins in autophagosome formation. *Annu Rev Cell Dev Biol.* 2011;27(1):107–132.
- [10] Chiang C, Gack MU. Post-translational control of intracellular pathogen sensing pathways. *Trends Immunol.* 2017;38(1):39–52.
- [11] Xie Y, Kang R, Sun X, et al. Posttranslational modification of autophagy-related proteins in macroautophagy. *Autophagy.* 2015;11(1):28–45.
- [12] Chen RH, Chen YH, Huang TY. Ubiquitin-mediated regulation of autophagy. *J Biomed Sci.* 2019;26(1):80.
- [13] Berndsen CE, Wolberger C. New insights into ubiquitin E3 ligase mechanism. *Nat Struct Mol Biol.* 2014;21(4):301–307.
- [14] Zheng N, Shabek N. Ubiquitin ligases: structure, function, and regulation. *Annu Rev Biochem.* 2017;86(1):129–157.
- [15] Deshaies RJ, Joazeiro CA. RING domain E3 ubiquitin ligases. *Annu Rev Biochem.* 2009;78(1):399–434.
- [16] Goto J, Otaki Y, Watanabe T, et al. The role of HECT-Type E3 ligase in the development of cardiac disease. *Int J Mol Sci.* 2021;23(1):22.

- [17] Yang Y, Zhu Y, Zhou S, et al. TRIM27 cooperates with STK38L to inhibit ULK1-mediated autophagy and promote tumorigenesis. *EMBO J.* 2022;41(14):e109777.
- [18] Xu C, Feng K, Zhao X, et al. Regulation of autophagy by E3 ubiquitin ligase RNF216 through BECN1 ubiquitination. *Autophagy.* 2014;10(12):2239–2250.
- [19] Chakraborty A, Diefenbacher ME, Mylona A, et al. The E3 ubiquitin ligase Trim7 mediates c-Jun/AP-1 activation by Ras signalling. *Nat Commun.* 2015;6(1):6782.
- [20] Lu M, Zhu X, Yang Z, et al. E3 ubiquitin ligase tripartite motif 7 positively regulates the TLR4-mediated immune response via its E3 ligase domain in macrophages. *Mol Immunol.* 2019;109:126–133.
- [21] Jin J, Lu Z, Wang X, et al. E3 ubiquitin ligase TRIM7 negatively regulates NF-kappa B signaling pathway by degrading p65 in lung cancer. *Cell Signal.* 2020;69:109543.
- [22] Zhu L, Qin C, Li T, et al. The E3 ubiquitin ligase TRIM7 suppressed hepatocellular carcinoma progression by directly targeting Src protein. *Cell Death Differ.* 2020;27(6):1819–1831.
- [23] Zhou C, Zhang Z, Zhu X, et al. N6-Methyladenosine modification of the TRIM7 positively regulates tumorigenesis and chemoresistance in osteosarcoma through ubiquitination of BRMS1. *EBioMedicine.* 2020;59:102955.
- [24] Fan W, Mar KB, Sari L, et al. TRIM7 inhibits enterovirus replication and promotes emergence of a viral variant with increased pathogenicity. *Cell.* 2021;184(13):3410–25 e17.
- [25] Yang B, Zhang G, Qin X, et al. Negative regulation of RNF90 on RNA virus-triggered antiviral immune responses targeting MAVS. *Front Immunol.* 2021;12:730483.
- [26] Yang B, Liu Y, Cui Y, et al. RNF90 negatively regulates cellular antiviral responses by targeting MITA for degradation. *PLoS Pathog.* 2020;16(3):e1008387.
- [27] Hansen K, Prabakaran T, Laustsen A, et al. *Listeria monocytogenes* induces IFN β expression through an IFI16-, cGAS- and STING-dependent pathway. *EMBO J.* 2014;33(15):1654–1666.
- [28] Collier JJ, Suomi F, Olahova M, et al. Emerging roles of ATG7 in human health and disease. *EMBO Mol Med.* 2021;13(12):e14824.
- [29] Kuang E, Qi J, Ronai Z. Emerging roles of E3 ubiquitin ligases in autophagy. *Trends Biochem Sci.* 2013;38(9):453–460.
- [30] Vittal V, Stewart MD, Brzovic PS, et al. Regulating the regulators: recent revelations in the control of E3 ubiquitin ligases. *J Biol Chem.* 2015;290(35):21244–21251.
- [31] Park Y, Jin HS, Aki D, et al. The ubiquitin system in immune regulation. *Adv Immunol.* 2014;124:17–66.
- [32] Liu X, Wang Q, Chen W, et al. Dynamic regulation of innate immunity by ubiquitin and ubiquitin-like proteins. *Cytokine Growth Factor Rev.* 2013;24(6):559–570.
- [33] Zhang W, Tan X, Lin S, et al. CPLM 4.0: an updated database with rich annotations for protein lysine modifications. *Nucleic Acids Res.* 2022;50(D1):D451–D9.
- [34] Feng Y, Yao Z, Klionsky DJ. How to control self-digestion: transcriptional, post-transcriptional, and post-translational regulation of autophagy. *Trends Cell Biol.* 2015;25(6):354–363.
- [35] Delcour C, Amazit L, Patino LC, et al. ATG7 and ATG9A loss-of-function variants trigger autophagy impairment and ovarian failure. *Genet Med.* 2019;21(4):930–938.
- [36] Marinho FV, Benmerzoug S, Oliveira SC, et al. The emerging roles of STING in bacterial infections. *Trends Microbiol.* 2017;25(11):906–918.
- [37] Ohsumi Y. Molecular dissection of autophagy: two ubiquitin-like systems. *Nat Rev Mol Cell Biol.* 2001;2(3):211–216.
- [38] Zheng H, Lu X, Li K, et al. ATG ubiquitination is required for circumsporozoite protein to subvert host innate immunity against rodent malaria liver stage. *Front Immunol.* 2022;13:815936.
- [39] Gomes LC, Dikic I. Autophagy in antimicrobial immunity. *Mol Cell.* 2014;54(2):224–233.
- [40] Castillo EF, Dekonenko A, Arko-Mensah J, et al. Autophagy protects against active tuberculosis by suppressing bacterial burden and inflammation. *Proc Natl Acad Sci U S A.* 2012;109(46):E3168–76.
- [41] Henault J, Martinez J, Riggs JM, et al. Noncanonical autophagy is required for type I interferon secretion in response to DNA-immune complexes. *Immunity.* 2012;37(6):986–997.
- [42] Lee HK, Mattei LM, Steinberg BE, et al. In vivo requirement for Atg5 in antigen presentation by dendritic cells. *Immunity.* 2010;32(2):227–239.
- [43] Mostowy S, Sancho-Shimizu V, Hamon MA, et al. p62 and NDP52 proteins target intracytosolic *Shigella* and *Listeria* to different autophagy pathways. *J Biol Chem.* 2011;286:26987–26995.
- [44] Wang J, Song D, Liu Y, et al. HLA-DMB restricts human T-cell leukemia virus type-1 (HTLV-1) protein expression via regulation of ATG7 acetylation. *Sci Rep.* 2017;7(1):14416.
- [45] Yang B, Wang J, Wang Y, et al. Novel function of Trim44 promotes an antiviral response by stabilizing VISA. *J Immunol.* 2013;190(7):3613–3619.
- [46] Wang J, Yang B, Hu Y, et al. Negative regulation of Nmi on virus-triggered type I IFN production by targeting IRF7. *J Immunol.* 2013;191(6):3393–3399.
- [47] Wang Y, Lian Q, Yang B, et al. TRIM30alpha is a negative-feedback regulator of the intracellular DNA and DNA virus-triggered response by targeting STING. *PLoS Pathog.* 2015;11(6):e1005012.
- [48] Lou Y, Han M, Liu H, et al. Essential roles of S100A10 in Toll-like receptor signaling and immunity to infection. *Cell Mol Immunol.* 2020;17(10):1053–1062.
- [49] Wang J, Kang L, Song D, et al. Ku70 senses HTLV-1 DNA and modulates HTLV-1 replication. *J Immunol.* 2017;199(7):2475–2482.
- [50] Yang B, Song D, Liu Y, et al. IFI 16 regulates HTLV-1 replication through promoting HTLV-1 RT1-induced innate immune responses. *FEBS Lett.* 2018;592(10):1693–1704.